An Aurora kinase A-BOD1L1-PP2A B56 Axis promotes chromosome segregation fidelity

Thomas J. Kucharski[1,2], Irma M. Vlasac[3], Martin R. Higgs[4], Brock C. Christensen[3,5,6,7], Susanne Bechstedt[2] and Duane A. Compton[1,6*]

1) Department of Biochemistry and Cell Biology, Geisel School of Medicine at Dartmouth

2) Department of Anatomy and Cell Biology, McGill University, Montréal, Canada, H3A 0C7

3) Department of Epidemiology, Geisel School of Medicine at Dartmouth

4) Institute of Cancer and Genomic Sciences, University of Birmingham, Birmingham, B15 2TT, UK

5) Department of Molecular and Systems Biology, Geisel School of Medicine at Dartmouth

6) Department of Community and Family Medicine, Geisel School of Medicine at Dartmouth

7) Dartmouth Cancer Center, Geisel School of Medicine at Dartmouth, Lebanon, NH

*Corresponding author

Keywords: kinetochore, microtubule, mitosis, phosphorylation, Aurora, phosphatase

Correspondence address:
Department of Biochemistry and Cell Biology
Geisel School of Medicine at Dartmouth
WTRB Level 6
1 Medical Center Drive
Lebanon, N.H. 03756
USA
603-650-1190 (phone)
603-650-1128 (FAX)
duane.a.compton@dartmouth.edu
geiselmed.dartmouth.edu/compton/

Word count for the summary:

Character count for the text: (no references, methods or figure legends)

Summary

Cancer cells are often aneuploid and frequently display elevated rates of chromosome mis-segregation in a phenomenon called chromosomal instability (CIN). CIN is commonly caused by hyperstable kinetochore-microtubule (K-MT) attachments that reduces the efficiency of correction of erroneous K-MT attachments. We recently showed that UMK57, a chemical agonist of MCAK (alias KIF2C) improves chromosome segregation fidelity in CIN cancer cells although cells rapidly develop adaptive resistance. To determine the mechanism of resistance we performed unbiased proteomic screens which revealed increased phosphorylation in cells adapted to UMK57 at two Aurora kinase A phosphoacceptor sites on BOD1L1 (alias FAM44A). BOD1L1 depletion or Aurora kinase A inhibition eliminated resistance to UMK57 in CIN cancer cells. BOD1L1 localizes to spindles/kinetochores during mitosis, interacts with the PP2A phosphatase, and regulates phosphorylation levels of kinetochore proteins, chromosome alignment, mitotic progression and fidelity. Moreover, the *BOD1L1* gene is mutated in a subset of human cancers, and *BOD1L1* depletion reduces cell growth in combination with clinically relevant doses of taxol or Aurora kinase A inhibitor. Thus, an Aurora kinase A -BOD1L1-PP2A axis promotes faithful chromosome segregation during mitosis. (175 words)

49 **Introduction**

50 Faithful chromosome segregation during cell division relies on proper bioriented
51 attachment of kinetochores to spindle microtubules. Errors in kinetochore-microtubule (k-MT)
52 attachment arise frequently during early phases of mitosis and the persistence of these errors is a
53 common cause of the elevated rate of chromosome mis-segregation resulting in chromosomal
54 instability (CIN) and aneuploidy in solid tumors [1–5]. We previously demonstrated that strategies
55 that destabilize k-MT attachments promote faithful chromosome segregation in CIN cancer cells
56 by increasing the correction rate of k-MT attachment errors. Specifically, overexpression of
57 either MCAK (alias KIFC) or KIF2B microtubule depolymerases suppressed chromosome mis-
58 segregation in a variety of CIN cancer cell lines[5–8]. These data demonstrate the potential of
59 suppressing CIN as a strategy for cancer treatment.

60 To pursue this strategy we recently characterized a cell-permeable small molecule agonist
61 of MCAK activity called UMK57. MCAK plays a key role at centromeres/kinetochores by
62 driving microtubule detachment to increase k-MT turnover to facilitate error correction prior to
63 anaphase[9,10]. At moderate dosage (100 nM), UMK57 increases the rate of k-MT detachment and
64 therefore decreases the rate of chromosome mis-segregation in anaphase. Surprisingly, high rates
65 of chromosome mis-segregation returned to CIN cancer cells after only ~72 hours of treatment
66 with UMK57. This resistance arose within the entire cell population, did not depend on the
67 activity of drug efflux pumps, did not occur due to a loss of drug activity, changes in the level or
68 localization of MCAK, or changes to overall spindle morphology, and data demonstrated that
69 MCAK activity continued to be activated by UMK57 in treated cells. Thus, this represents
70 adaptive resistance (as opposed to acquired resistance which relies on the emergence of rare

71 genetic variants) to UMK57 whereby changes to cell signaling pathways bypass increased
72 MCAK activity.
73 To determine the mechanisms by which CIN cancer cells develop resistance to UMK57,
74 we performed unbiased proteomic screens using mass spectrometry to identify changes in total
75 protein and protein phosphorylation levels between acutely treated and adapted cells in mitosis.
76 These screens revealed changes in phosphorylation of two Aurora kinase A sites in the C-
77 terminus of the large nuclear protein BOD1L1. Subsequent studies revealed that both Aurora
78 kinase A activity and BOD1L1 expression are required for cellular resistance to prolonged
79 UMK57 treatment. Moreover, BOD1L1 localizes to the mitotic spindle and kinetochores,
80 interacts with the Protein Phosphatase 2 (PP2A) complex and is required for setting correct
81 levels of kinetochore phosphorylation to support faithful chromosome segregation. Therefore,
82 cells rely on an Aurora kinase A-BOD1L1-PP2A axis to maintain proper k-MT attachment
83 stability for faithful chromosome segregation and utilize this axis to alter kinetochore
84 phosphorylation as a mechanism to adapt to persistent k-MT destabilization. Importantly,
85 BOD1L1 mutation is associated with improved prognosis in uterine endometrial cancer.
86 Accordingly, we show that loss of BOD1L1 expression reduces cellular fitness of cancer cell
87 lines in culture and induces catastrophic levels of chromosome mis-segregation in combination
88 with taxol and Aurora kinase A inhibitor.
89

90 **Results**

91 Proteomic analysis of UMK57 resistance in mitotic cells

92 To investigate the cellular mechanisms promoting resistance to UMK57, we developed
93 conditions for proteomic screens in mitotic cells (Figure 1A). We utilized SW620 (lymph node
94 metastasis of colon cancer) cells for this purpose because they are CIN and they undergo
95 adaptive resistance to UMK57[11]. Specifically, SW620 cells naïve to UMK57 display lagging
96 chromosomes in 34% of anaphases, on average. The rate of lagging chromosomes in anaphase
97 decreases to 25% upon treatment with 100nM UMK57 for 1 hour, and rebounds to 37%
98 following 72 hours continuous treatment (Figure 1B). SW620 cells also display reduced
99 phosphorylation of MCAK pS95 and Aurora kinase B pT232 following 72 hours continuous
100 treatment with UMK57 consistent with our previous findings indicating that changes in
101 centromere/kinetochore phosphorylation levels correlated with the adaptive resistance response
102 (Figure S1A-D). Therefore, SW620 cells likely adapt to UMK57 by altering signaling networks
103 leading to changes in the phosphorylation of specific kinetochore proteins, as suggested
104 previously[11].

105 For proteomic analysis, we first treated SW620 cells with 100nM UMK57 for 72 hours to
106 represent the adapted condition. A parallel set of cells was treated with DMSO for 72 hours. The
107 cells were then synchronized by thymidine-nocodazole (still in the presence of DMSO/UMK57)
108 followed by 1 hour treatment of the DMSO population with 100nM UMK57 immediately prior
109 to harvest to represent the acutely treated condition. Mitotic cells were harvested by shake-off
110 and compared for differences in total protein level and protein phosphorylation level by mass
111 spectrometry (Figure 1A).

112 For comparison of total protein levels, we obtained data for 6966 proteins based on 7704
113 unique and 150981 total peptides (Figure 1C). Among these, protein levels between the two cell
114 populations varied from +1.725 to 0.41-fold change with 6813 proteins (97.7%) varying between
115 the two cell populations within +1.2 and 0.8-fold-change. Protein levels skewed towards
116 increased levels in one biological replicate resulting in a skewed overall distribution (Figure S1E,
117 supplemental table 1). Among the proteins identified, the levels of Sgo2 were significantly
118 increased (#38, +1.30-fold, $p = 0.0037$, 6 peptides) in adapted cells. Sgo2 is an interesting
119 candidate for involvement in UMK57 adaptation as it is extensively implicated in setting
120 kinetochore phosphorylation levels[12,13]. However, independent validation of a change in Sgo2
121 protein level by immunoblot was inconclusive (Figure S2F). The catalytic subunit of PP2A
122 (PPP2CB) appeared to be decreased in protein level in adapted cells, although that was based on
123 a single peptide and so was discarded (supplemental table 1). Thus, total protein levels in mitotic
124 SW620 cells that have adapted to UMK57 change very little, and generally within a narrow
125 range, relative to mitotic SW620 cells that are acutely treated with UMK57.
126 We next examined the phospho-proteomic changes in mitotic SW620 cells that have
127 adapted to UMK57 versus cells that are acutely treated. We obtained data from 47,550 unique
128 peptides from 122241 total peptides. Of these, 31,563 sites were quantified, and 23,155 sites
129 were both quantified and localized (Figure 1C, supplemental table 2). Among these, phospho-
130 peptide levels between the two cell populations varied from 2.98 to 0.27-fold change with 19973
131 (86.2%) varying between the two cell populations within 1.2 to 0.8-fold-change. 6378 phospho-
132 peptides displayed an increased abundance in UMK57 adapted cells and 16777 peptides showed
133 decreased abundance.

134 We performed Gene ontology analysis on the group of proteins that displayed significant
135 changes in peptide phosphorylation ($p < 0.1$). We included both proteins showing increases or
136 decreases in protein phosphorylation to capture changes caused by altered kinase or phosphatase
137 activity. This analysis revealed significant over-representation of proteins involved in mitotic
138 processes including chromosome condensation, centromere/chromosome localization, and
139 microtubule polymerization and de-polymerization, consistent with an adaptive resistance to
140 UMK57 altering mitotic processes including microtubule dynamics (Figure 1D). STRING
141 protein-protein interaction network analysis of the top and bottom 100 proteins displaying the
142 largest, significant changes in peptide phosphorylation revealed a cluster of proteins involved in
143 mitosis. Of these, proteins with peptides displaying significantly increased levels of
144 phosphorylation in adapted cells relative to acutely treated cells include Numa, 53BP1, Ska3,
145 INCENP and BOD1L1 (Alias FAM44A). Proteins with peptides displaying significantly
146 decreased levels of phosphorylation in adapted cells relative to acutely treated cells included
147 Knl1, Numa, Hec1, NUSAP, INCENP and TPX2 (Figure 1F, supplemental table 2). Thus, our
148 dataset contains proteins whose phosphoregulation might plausibly mediate adaptation to
149 UMK57.
150 Analysis of the amino acid sequences of the potential phosphoacceptor sites identified in
151 the screen with significant changes in phosphorylation level ($p<0.1$) shows over-representation
152 of the canonical Cdk phosphorylation site motif (S/TPxxK) and possibly Aurora kinase motifs
153 (R/KR/KxS/T) (Figure 1E). We explored if there was enrichment of Aurora substrates in our
154 dataset utilizing a previous screen that identified many Aurora-dependent phosphoacceptors sites
155 in mitosis[14] and that categorized peptides as being selectively phosphorylated by either Aurora
156 kinase A or Aurora kinase B using selective chemical inhibitors of those kinases. This analysis

157 revealed a 10.1- and 12.6-fold over-representation of Aurora kinase A substrates and Aurora
158 kinase B substrates, respectively, among the population of phosphoacceptors sites identified in
159 our dataset, although many phosphoacceptors sites could be phosphorylated by both kinases
160 (Figure 1G).

161 Among all proteins that displayed changes in phosphorylation level in adapted cells
162 relative to acutely treated cells, BOD1L1 demonstrated the most significant change. 32 different
163 BOD1L1 phospho-peptides were detected in the phospho-proteomic screen, of which 3 showed
164 statistically significant positive changes, and two statistically significant negative changes.
165 BOD1L1 (FAM44A) is closely related to Bod1 (FAM44B) and Bod1L2 (FAM44C), but
166 contains a short proline rich n-terminal extension, and a long, c-terminal extension (Figure 1H).
167 Of note, one BOD1L1 peptide was doubly phosphorylated on T2956 and S2958 and displayed a
168 significant increase (1.3-fold; $p = 0.06$) in phosphorylation in adapted cells relative to acutely
169 treated cells. Another peptide was also doubly phosphorylated and contains S2973 and 2986 and
170 displayed a significant increase (2.3-fold; $p < 0.01$) in phosphorylation in adapted cells relative
171 to acutely treated cells. Another peptide was singly phosphorylated at S2986 and displayed a
172 significant increase (1.2-fold; $p = 0.07$) in phosphorylation in adapted cells relative to acutely
173 treated cells. Importantly, the total protein level of BOD1L1 did not change in adapted cells
174 relative to acutely treated cells (1.06-fold; $p = 0.26$; 15 peptides) (Figure 1F, supplemental table
175 1) indicating that BOD1L1 undergoes net changes in phosphorylation status as cell adapt to
176 UMK57. The peptide containing S2954, T2956 and S2958 was previously identified in a
177 phospho-proteomic screen[14], and the conserved cluster of lysine and arginine residues proximal
178 to the phosphoacceptors sites suggest phosphorylation by Aurora kinases (figure 1I). Indeed,
179 previous proteomic analysis demonstrated that phosphorylation of this peptide is sensitive to an

180 Aurora kinase A inhibitor in a dose-dependent manner, and insensitive to an inhibitor of Aurora
181 kinase B (Figure S1H)[14]. Moreover, BOD1L1 was previously detected in an Aurora kinase A
182 proximity-ligation mapping experiment[15]. These data indicate that BOD1L1 is selectively
183 phosphorylated by Aurora kinase A as cells adapt to UMK57. Interestingly, BOD1L1 is
184 distinguished from other members of this gene family because neither Bod1 nor Bod1L2 contain
185 obvious Aurora kinase consensus sites and the phosphoacceptors sites identified here and in
186 previous proteomic screens are in the extended c-terminal domain that is unique to BOD1L1, in
187 agreement with the fact that BOD1L1 is functionally distinct from BOD1 during DNA repair[16].
188

189 <u>BOD1L1 and Aurora kinase A are required for adaptation to UMK57</u>

190 To determine if BOD1L1 is functionally required for adaptive resistance to UMK57 in
191 CIN cancer cells, we used two independent shRNA sequences to knockdown BOD1L1
192 expression and selected cells for shRNA expression using puromycin treatment. We confirmed a
193 durable knockdown of BOD1L1 over several days in cells expressing BOD1L1 shRNA
194 compared to cells expressing control shRNA using BodlL1-specific antibodies on immunoblot
195 and through indirect immunofluorescence. (Figure S2A, S2B).

196 Next, we tested if BOD1L1 is required for cells to adapt to UMK57. We transfected cells
197 with BOD1L1-specific shRNA or control shRNA expressing plasmids, selected for puromycin
198 resistance, added UMK57 for short or prolonged periods and then measured the frequency of
199 lagging chromosomes during mitosis. As expected in cells transfected with control shRNA, acute
200 treatment with UMK57 reduces the frequency of lagging chromosomes in anaphase and high
201 lagging chromosome rates return upon prolonged treatment with UMK57. Cells transfected with
202 either of two distinct BOD1L1 shRNA's display elevated rates of lagging chromosomes in

203 anaphase compared to cells transfected with control shRNA. Despite the identified role for
204 BOD1L1 in DNA repair, the increased rate of lagging chromosomes that we observe in BOD1L1
205 knockdown cells is not likely due to elevated levels of DNA damage, as it was previously
206 demonstrated that there is no increase in basal levels of DNA repair foci in knockdown cells
207 compared to control cells in the absence of prior cell irradiation[17]. BOD1L1-deficient cells
208 respond to acute treatment with UMK57 and show significantly fewer anaphase cells with
209 lagging chromosomes. The effect of UMK57 on BOD1L1-deficient cells is durable because cells
210 retain significantly reduced lagging chromosome rates compared to DMSO-treated cells
211 throughout prolonged treatment (Figure 2A, 2B). Therefore, BOD1L1 expression is required for
212 adaptation to prolonged UMK57 treatment.

213 Since BOD1L1 is phosphorylated by Aurora kinase A in mitosis and there was a
214 significant increase in BOD1L1 phosphorylation during adaptation to prolonged UMK57
215 treatment, we also tested if Aurora kinase A activity is required for adaptation to UMK57. We
216 treated cells concurrently with a sublethal 50 nM dose of Aurora kinase A inhibitor and UMK57
217 over 3 days and assessed the rates of lagging chromosomes. SW620 cells continued to proliferate
218 in the presence of this dose of Aurora kinase A inhibitor (Figure S2C), and cells treated with
219 Aurora kinase A inhibitor alone displayed elevated levels of lagging chromosomes compared to
220 cells treated with DMSO. Cells treated with Aurora kinase A inhibitor respond to acute treatment
221 with UMK57 and display significantly fewer lagging chromosomes in anaphase relative to cells
222 treated with the Aurora kinase A inhibitor alone. The fraction of anaphase cells with lagging
223 chromosomes remained significantly reduced in cells with prolonged UMK57 treatment when
224 Aurora kinase A was inhibited demonstrating that Aurora kinase A is also required for adaptation
225 to prolonged UMK57 treatment (Figure 2C).

226 These and previous data[11] indicate that adaptation to prolonged UMK57 treatment likely
227 occurs through changes in kinetochore protein phosphorylation and that BOD1L1 may play a
228 role in regulating protein phosphorylation. Therefore, we tested if treatment of cells with a
229 modest dose of Okadaic acid[18], which inhibits PP2A and to a lesser extent PP1 phosphatases,
230 would alter the rate of lagging chromosomes in anaphase. Cells transfected with control shRNA
231 displayed a reduced frequency of lagging chromosomes in anaphase when treated with Okadaic
232 acid, suggesting that elevated protein phosphorylation can increase chromosome segregation
233 fidelity (Figure 2D). As expected, BOD1L1-deficient cells display elevated numbers of lagging
234 chromosomes in anaphase. Remarkably, cells transfected with shRNA against BOD1L1 and
235 treated with Okadaic acid had rates of lagging chromosomes in anaphase that were not different
236 from control shRNA/DMSO treated cells. Thus, Okadaic acid treatment effectively replaces
237 BOD1L1 function in mitosis as measured by chromosome segregation fidelity indicating that
238 BOD1L1 likely acts as a negative regulator of protein phosphatase activity and that the elevated
239 rate of lagging chromosomes in BOD1L1-deficient cells (Figure 2A) is due to reduced levels of
240 protein phosphorylation.
241 Since Aurora kinase A is required for adaptation to UMK57, we used cell biological
242 approaches to test if Aurora kinase A activity is altered in cells treated either acutely with or
243 adapted to UMK57. We measured the intensity of Aurora kinase A and pT288 Aurora kinase A,
244 a marker of Aurora kinase A activity in mitotic cells from an asynchronous culture. Whereas the
245 ratio of Aurora kinase A to pT288 Aurora kinase A remained unchanged in cells treated acutely
246 with or adapted to UMK57 compared to control cells (i.e., no change in phospho-occupancy), the
247 overall levels of both Aurora kinase A and pT288 Aurora kinase A on mitotic spindles strongly
248 increased in cells treated with UMK57 (Figure 3A, 3B). Since TPX2 directs Aurora kinase A to

249 the mitotic spindle[19], we quantified the levels of TPX2 and alpha tubulin in the mitotic spindle in
250 cells treated with UMK57. Similar to Aurora kinase A, this experiment revealed elevated levels
251 of TPX2 on the mitotic spindle in cells treated with UMK57 despite a decrease in overall levels
252 of spindle microtubule content in treated cells (Figure 3C, 3E). TACC3, another spindle-
253 associated protein, displayed spindle intensity that roughly mirrored the levels of spindle
254 microtubule content (Figure 3D, 3E) indicating that the quantity of Aurora kinase A and TPX2
255 on spindles selectively increased upon UMK57 treatment.
256
257 BOD1L1 regulates mitotic progression and mitotic fidelity
258 To date, the only role identified for BOD1L1 is in DNA repair[16,17,20]. BOD1L1 shares
259 extensive sequence similarity to Bod1 which has been shown to be involved in regulation of
260 mitotic activities including kinetochore protein phosphorylation by recruiting the PP2A-B56
261 phosphatase, regulating MCAK localization, and also to be important for chromosome
262 alignment[21–23]. Given the similarities between Bod1 and BOD1L1, and that BOD1L1-deficient
263 cells display increased rates of lagging chromosomes in anaphase and that BOD1L1 function in
264 mitotic fidelity can be rescued using protein phosphatase inhibitors, we focused our efforts on
265 understanding the contribution of BOD1L1 to mitotic processes and chromosome segregation
266 fidelity.
267 Using immunofluorescence microscopy we detected BOD1L1 at spindle poles, on
268 microtubules and at kinetochores of SW620 cells (Figure 4A, 4B). Line scans showed significant
269 overlap between BOD1L1 and Hec1 at kinetochores in prometaphase through anaphase.
270 Notably, BOD1L1 does not localize to all kinetochores, but rather to a subset, suggesting the
271 possibility of regulation of BOD1L1 localization. Since BOD1L1 localizes to the mitotic spindle,

272 we also examined if BOD1L1 co-localizes with Aurora kinase A. We found a large degree of co-
273 localization between Aurora kinase A and BOD1L1 at the spindle poles and along pole-proximal
274 microtubules (Figure 4C). BOD1L1 co-localized with Hec1 on kinetochores in cells treated with
275 either a low or high dose of nocodazole demonstrating that BOD1L1 does not require
276 microtubules for kinetochore localization (Figure S2D). BOD1L1 localization was also
277 unchanged by treatment of cells with Aurora kinase A or Aurora kinase B inhibitors
278 demonstrating that BOD1L1 kinetochore localization is independent of these kinase activities
279 despite the problems in spindle structure and chromosome alignment caused by these inhibitors
280 (Figure S2E).

281 BOD1L1-deficient cells appear to have aberrant spindle structures and problems with
282 chromosome alignment. We quantified these phenotypes by measuring the proportion of cells in
283 each phase of mitosis as a percentage of all mitotic cells. BOD1L1-deficient early prometaphase
284 cells often had small spindles with kinetochores located close to the poles, whereas late
285 prometaphase cells had difficulties in chromosome alignment (Figure 5A, 5B), with many
286 chromosomes located proximal to the spindle poles. We also used time-lapse microscopy on
287 mCherry-H2B expressing SW620 cells to measure the time spent in mitosis with and without
288 BOD1L1. Control cells needed on average 57 minutes to transit mitosis from the onset of
289 chromosome condensation to anaphase. In contrast, BOD1L1-deficient cells spent on average
290 208.3 minutes (shRNA #1) and 120.6 minutes (shRNA #2) in mitosis. These changes in the
291 average time taken to complete mitosis overestimates the overall impact of mitotic delay in
292 BOD1L1-deficient cells because it is skewed by cells that either underwent slippage or death
293 following extended times in mitosis. Amongst cells that completed mitosis with anaphase, these

294 cells took an average of 137.5 (shRNA #1) and 100.0 minutes (shRNA #2) to transit mitosis
295 (Figure 5C, S3A). Thus, BOD1L1 is functionally required for efficient mitotic progression.
296 Next, we tested if BOD1L1 contributes to k-MT attachment stability. Following
297 transfection with control or BOD1L1-specific shRNA plasmids and puromycin selection, we
298 cold treated cells to eliminate non-k-MT from spindles and fixed and stained cells for tubulin and
299 ACA. The spindle microtubule intensity in BOD1L1-deficient cells was increased in both
300 prometaphase and metaphase relative to cells transfected with control shRNA (Figure 5D, E).
301
302 BOD1L1 interacts with the PP2A-B56 phosphatase and regulates kinetochore phosphorylation
303 To gain further insight into the role(s) of BOD1L1 in mitosis, we immunoprecipitated
304 BOD1L1 from mitotic cells to determine the identity of interacting proteins. We cross-linked
305 antibody to protein G beads and used them to immunoprecipitate BOD1L1 interacting proteins
306 from SW620 cells synchronized in mitosis through sequential treatment with thymidine and
307 nocodazole. The eluted proteins were then separated by SDS-PAGE gel, stained with Coomassie,
308 cut into fractions and analyzed by mass spectrometry (Figure 6A). This analysis revealed a high
309 affinity interaction with the MTORC2 signaling complex which regulates cellular pro-survival
310 and is typified by the presence of the Rictor protein subunit[24] as judged by the very high number
311 of detected peptides. Also, there were numerous mRNA translation initiation factor proteins, and
312 abundant peptides from the CCT chaperone complex. In addition, we detected several proteins
313 that participate in DNA repair, including SETD1A, RAD50, XRCC5, XRCC6, RIF1 and
314 MRE11, consistent with previous findings, and which serve as positive controls for the
315 specificity of our assay[17,20]. We also detected various core subunits of the Anaphase Promoting
316 Complex/Cyclosome, although we did not detect the co-activator proteins Cdh1 or Cdc20. Thus,

317 BOD1L1 may be an APC/C substrate or a regulator of APC/C activity. We also detected
318 numerous proteins with documented mitotic functions including Sgo2, CENPF, MCAK, Numa,
319 Aurora kinase A, and several components of the PP2A-B56 phosphatase complex including both
320 PPP2R1A and PPP2R1B regulatory subunits, the PPP2CA catalytic subunit, and the PPP2R5E
321 epsilon adaptor subunit (Figure 6B, Supplemental table 3). Therefore, like Bod1, BOD1L1
322 interacts with PP2A and likely regulates PP2A activity or is itself regulated by PP2A. These
323 interacting proteins were independently validated by blotting for various proteins. We detected
324 the PP2A catalytic, regulatory and the delta, gamma, and epsilon adaptor subunits, but not the
325 beta subunit. We also detected CENPF, MCAK, Bub3, SMC1 and APC3 proteins in BOD1L1
326 immunoprecipitates (Figure 6C). These interactions were generally enriched when BOD1L1 was
327 immunoprecipitated from cells synchronized in mitosis, compared to asynchronous cells.
328 There are notable similarities and differences in the interactomes of Bod1 and
329 BOD1L1[23]. Like Bod1, BOD1L1 interacts with PP2A-B56, SMC1A, SMC3, SETD1A, Aurora
330 kinase A and Bub3. In contrast, Bod1 did not show interaction with the MTORC2 complex, but
331 does interact with Hec1, Knl1 and components of the fibrous corona including Zwint, ZW10 and
332 dynein. Hec1 is among the strongest interacting proteins with Bod1 but was not detected as an
333 interactor with BOD1L1 in our analysis despite the co-localization of BOD1L1 with Hec1 at
334 kinetochores at the resolution of immunofluorescence microscopy. To test directly if BOD1L1
335 kinetochore localization requires Hec1, we utilized HeLa cells with doxycycline inducible
336 CRISPR/Cas9 Hec1 genetic knockout[25], and compared the localization of BOD1L1 in the
337 presence and absence of Hec1. We did not detect a significant change in BOD1L1 localization
338 indicating that Hec1 is not required for BOD1L1 kinetochore localization (Figure S3B).

339 To determine which domain of BOD1L1 is responsible for interaction with the PP2A
340 complex, we performed a pull-down experiment using fragments of BOD1L1 fused to GST as
341 bait from lysates of mitotic SW620 cells. Surprisingly, despite the high degree of similarity
342 between the n-terminus of BOD1L1 and Bod1 and the fact that both Bod1 and BOD1L1 interact
343 with PP2A subunits, the region of BOD1L1 that bound to the PP2A complex most strongly was
344 the uncharacterized central domain from amino acid 500 to 2001. Additionally, the c-terminal F6
345 fragment also interacted with the PP2A B56 delta subunit (Figure 6D). In contrast, it is the n-
346 terminal F1-F2 Bod1-similar and C-terminal F6 regions that bind Rif1 in the context of the DNA
347 damage response[17].
348 These data indicate that BOD1L1 might regulate the PP2A-B56 complex during mitosis
349 to regulate mitotic fidelity. Therefore, we tested whether BOD1L1 regulates kinetochore protein
350 phosphorylation levels in a similar manner to Bod1. Using immunofluorescence, we quantified
351 the staining intensity for numerous phosphorylated proteins at kinetochores following depletion
352 of BOD1L1. We stained cells for Aurora kinase A pT288 (Aurora kinase A), Hec1 pS55 (Aurora
353 kinase A), Hec1 pT31 (Cdk1-Cyclin B1), Hec1 pS44 (Aurora kinase B), Dsn1 pS100 (Aurora
354 kinase B), Knl1 pMELT (Mps1), Aurora kinase B pT232 (Aurora kinase B) and MCAK pS95
355 (Aurora kinase B). We observed that the intensity of staining for Hec1 pS55, Hec1 pT31, Hec1
356 pS44, pDsn1 pS100, and Knl1 pMELT decreased in both prometaphase and metaphase and
357 Aurora kinase B pT232 levels decreased in prometaphase in BOD1L1-deficient cells. In contrast,
358 MCAK pS95 staining intensity increased in metaphase cells (Figure 7). Notably, we did not
359 detect a pattern of changes for Aurora kinase A pT288, indicating that total Aurora kinase A
360 activity levels are essentially unchanged in BOD1L1-deficient mitotic cells. To verify that the
361 observed changes in kinetochore protein phosphorylation were directly caused by loss of

362 BOD1L1, we transfected SW620 BOD1L1-knockdown cells with a plasmid to express GFP-
363 BOD1L1 and quantified the level of Hec1-pT31 and KNL1-pMELT during mitosis. There is a
364 detectable increase in BOD1L1 expression in cells expressing GFP-BOD1L1 although the
365 molecular weight change of the fusion protein is essentially unresolvable from endogenous
366 because of the very large molecular weight of BOD1L1 (>330k). The expression of GFP-
367 Bod1L1 restored Hec1 an KNL1 phosphorylation levels on these phosphoacceptors sites in the
368 knockdown cells and slightly increased the relative phosphorylation levels compared to control
369 cells (Figure S4A,B,C,F,G). Furthermore, to confirm BOD1L1 mitotic function in non-
370 transformed cells, we knocked down BOD1L1 with two independent shRNA sequences in the
371 non-tranformed and diploid cell line RPE1 and quantified the level of Hec1-pT31 and KNL1-
372 pMELT during mitosis. Transfection with either shRNA sequence induced a significant
373 reduction in the relative phosphorylation levels of Hec1 and KNL1 in RPE1 cells compared to
374 control cells consistent with observations in the transformed SW620 cells (Figure S4D,E,H,I).
375 These results combined with previous data showing that phosphatase inhibitors can rescue
376 lagging chromosomes in BOD1L1-deficient mitotic cells demonstrate that BOD1L1 functions as
377 a negative regulator of protein phosphatase activity to support efficient mitotic progression.
378 Consistently, the loss of BOD1L1 affects phospho-substrates at kinetochores that are
379 phosphorylated by multiple distinct protein kinases.
380
381 *BOD1L1* gene is mutated in human cancers
382 Since aneuploidy is associated with cancer development and BOD1L1-deficiency
383 increases mitotic error rates, we examined whether BOD1L1 is mutated in human cancers. We
384 queried The Cancer Genome Atlas (TCGA) for cancers that have somatic alterations in the wild-

385 type sequence in *BOD1L1*. Among the 10967 cancers that have been sequenced, 3.9% of cancers
386 show alterations in *BOD1L1* sequence, although the prevalence of *BOD1L1* alterations was
387 variable across cancer types. The five cancers with the highest percentage of *BOD1L1* somatic
388 alterations are uterine endometrial carcinoma (12.9%), lung adenocarcinoma (8.8%), skin
389 cutaneous melanoma (7.9%), stomach adenocarcinoma (7.7%) and lung squamous cell
390 carcinoma (6.6%). Because our data demonstrate that BOD1L1 is activated by Aurora kinase A
391 and functionally regulates PP2A activity, we also examined the TCGA for cancers that have
392 alterations in any of *BOD1L1*, *AURKA, TPX2, PPP2CA, PPP2CB, PPP2R1A, PPP2R1B,*
393 *PPP2R5A, PPP2R5B, PPP2R5C, PPP2R5D, PPP2R5E*. Surprisingly, 59.6% of uterine
394 carcinosarcoma and 43.9% of uterine endometrial cancers have alterations in one or more of
395 these genes, suggesting that genes in this biochemical pathway might be particularly relevant in
396 these cancer types (Figure S5A). We next tested associations of *BOD1L1* alteration with 5-year
397 overall survival adjusting for potential confounders in these patients. *BOD1L1* alteration was
398 significantly associated with improved 5-year survival in uterine cancer HR = 0.37 (95% CI:0.16
399 – 0.85). *BOD1L1* alteration was significantly associated with reduced 5-year survival in lung
400 adenocarcinoma HR = 1.66 (95% CI: 1.03-2.66) and in melanoma HR = 1.79 (95% CI: 1.07-
401 3.00). *BOD1L1* alteration did not demonstrate a significant association with patient survival in
402 stomach adenocarcinoma or lung squamous cell carcinoma (Figure 8B).
403 Given that BOD1L1 appears to function in a pathway consisting of Aurora kinase A-
404 BOD1L1-PP2A B56, we asked if individuals with mutations in *BOD1L1* also have co-occurring
405 mutations in either *AURKA* or its cofactor *TPX2* or in *PP2A* complex components. Using data
406 from the TCGA-PanCancer Atlas (n = 10,967), we observed that *BOD1L1* alterations were
407 exclusive of alterations to other *AURKA-BOD1L1- PP2A* gene pathway members. This was true

408 when testing *BOD1L1* alteration versus alteration to any other gene pathway member (Fisher's
409 exact P=1.3E-24), and *BOD1L1* alteration versus each of the eleven gene pathway members
410 independently (all Fisher's exact P<5.7E-08) (Figure S5B, S5C), suggesting that mutations in
411 multiple components of this pathway are not tolerated in cancers.

412 To understand how BOD1L1 inactivation affects cell proliferation and response to anti-
413 mitotic drugs including Aurora kinase A inhibitors or taxol, we compared the proliferation of
414 cells derived from various tumor types [U2OS (osteosarcoma), HCT116 (colorectal carcinoma),
415 SW620 (colorectal adenocarcinoma), HeLa (cervical adenocarcinoma) and HEC1 (uterine
416 endometrial adenocarcinoma)] following transfection with either control shRNA or BOD1L1-
417 specific shRNA. All of these cell lines express detectable BOD1L1, albeit at different levels, and
418 they all require BOD1L1 for mitotic fidelity because there was a significant increase in lagging
419 chromosome rates in all cell lines following shRNA-mediated depletion of BOD1L1. (Figure
420 S5D & S5E). All cell types tested have reduced proliferation following transfection with the
421 BOD1L1-specific shRNA compared to the control shRNA, although the magnitude of the
422 reduction varied between cell types. This variance was not proportional to the level of BOD1L1
423 expression (e.g. HEC1 and SW620 cells have comparable expression levels, but different
424 BOD1L1 sensitivities) (Figure 8C, 8D, S5D, S5G). The proliferation of these cells following
425 treatment with taxol and Aurora kinase A inhibitor also varied. Proliferation of HCT116 cells
426 was modestly reduced by depletion of BOD1L1, but profoundly suppressed by treatment with
427 either dose of either drug with or without BOD1L1. In contrast, there was a dose-dependent
428 reduction in proliferation of U2OS, HeLa, HEC1 and SW620 cells in response to each drug.
429 When combined with BOD1L1 deficiency, the lower dose of each drug caused a substantial
430 further reduction in cell proliferation in U2OS cells, while HeLa cells were less affected and

431 SW620 cells were not affected by the combination of BOD1L1 knockdown and taxol or Aurora
432 kinase A inhibitor (Figure 8C, 8D, S5G). In line with the differential toxicity that we observed,
433 U2OS cells with BOD1L1 knockdown formed micronuclei at a higher rate compared to control
434 cells, while in SW620 cells there was no difference in micronuclei formation between control
435 and BOD1L1 knockdown conditions (Figure S5F). Thus, the relative impact of BOD1L1 gene
436 alteration on patient cancer survival is variable which is mirrored by a variable impact on
437 proliferation of various cancer cell types following BOD1L1 depletion.
438 Finally, we tested the effect of BOD1L1 knockdown on the growth and sensitivity to
439 taxol and Aurora kinase A inhibitor in non-transformed, diploid RPE1 cells. Immunoblots verify
440 that the knockdown of BOD1L1 with each shRNA sequence was highly efficient (Figure S6A).
441 Nevertheless, the knockdown of BOD1L1 did not sensitize RPE1 cells to taxol or the Aurora
442 kinase A inhibitor at the dosages used. Indeed, RPE1 cells were more sensitive to taxol
443 treatment than to the knockdown of BOD1L1, and they were not sensitive to the Aurora A kinase
444 inhibitor (Figure S6).
445

446 **Discussion**

447 Using an unbiased proteomic screen, we have discovered a pathway that regulates mitotic
448 fidelity by controlling phosphatase activity directed at kinetochore substrates. In an unperturbed
449 mitosis, BOD1L1 binds and inhibits PP2A-B56, helping to maintain moderate levels of
450 phosphorylation of kinetochore substrates, thus decreasing k-MT attachment stability and
451 ultimately supporting mitotic progression and high chromosome segregation fidelity. We
452 envision a scenario that when CIN cancer cells are treated for prolonged periods with UMK57 to
453 destabilize k-MT attachments, the adaptation response involves an increase in recruitment of
454 Aurora kinase A to spindles through TPX2 which increases phosphorylation of BOD1L1 and
455 relieves the negative regulation of PP2A activity. Relief of this constraint on PP2A leads to
456 reduced phosphorylation of numerous kinetochore substrates at the k-MT interface which
457 restores hyperstable k-MT stability and resumes the CIN phenotype (Figure 8E). This
458 mechanism for adaptation to UMK57 is consistent with data showing that small changes in
459 kinetochore phosphorylation can cause large changes in chromosome segregation fidelity[26–28],
460 and that the mechanism of adaptation is independent of the continued functional impact of
461 UMK57 to activate MCAK[11]. Interestingly, it has been shown recently that cells adapt to
462 oncogenic RAS/MAPK signaling by becoming increasingly dependent on BubR1/PP2A. This is
463 because signaling through RAS/MAPK results in hyperactivity of mitotic kinases, reducing k-
464 MT stability and increasing dependence on BubR1/PP2A to maintain viable levels of
465 phosphorylation[29]. Thus, deregulation of phosphatase activity toward kinetochores substrates
466 appears to be a common cellular response to pathways that change mitotic fidelity.

467 In support of our observations, the gene *cell proliferation regulating inhibitor of protein*
468 *phosphatase 2A (CIP2A)* is fourth on the list of *BOD1L1* co-dependent genes from the CRISPR

469 screens displayed in the Cancer Dependency Map Project[30,31]. CIP2A is a functional oncogene
470 that inhibits the PP2A complex in various contexts including the DNA damage response, mitotic
471 entry and mitotic progression by replacing the structural subunit of the PP2A complex, blocking
472 phosphatase function[32,33]. Thus, the co-dependency between the two genes suggests that cell
473 lines that are dependent on BOD1L1 for regulating phosphatase activity do not tolerate the loss
474 of another gene that negatively regulates PP2A.

475 Notably, despite sharing a conserved domain, BOD1L1 and Bod1 do not bind PP2A
476 through the same region. Our data show that BOD1L1 binds to PP2A with the middle and c-
477 terminus of the protein which are not conserved in Bod1 (Figure 6D). Therefore, although the
478 PP2A regulating function of Bod1 and BOD1L1 is conserved[22], the mechanism of their
479 interaction with PP2A is not. In addition, BOD1L1 has gained the ability to regulate DNA repair
480 through binding Rif1 at the n-terminus[17] and shifted the PP2A binding region to a large middle
481 region of the protein plus the c-terminus. This genetic separation of DNA damage and PP2A
482 regulating functions might explain the long c-terminal extension present in BOD1L1 compared
483 to Bod1 and Bod1L2. Importantly, the phosphoacceptor sites on BOD1L1 that increase
484 phosphorylation during the adaptation response to UMK57 also reside in the c-terminal domain
485 of the protein and are not conserved with Bod1. Thus, the regulation of BOD1L1 by Aurora
486 kinase A phosphorylation is distinct from processes that regulate Bod1.

487 A prevailing model differentiating the functional roles of Aurora A and B kinases in
488 mitosis is that although they both use the same consensus motif to recognize substrates, their
489 impact is different because they are spatially separated, with Aurora kinase A residing at spindle
490 poles and on microtubules, and Aurora kinase B at centromeres. Although compelling, this
491 model continues to be refined based on recent findings that some or perhaps even most non-CDK

492 phosphorylation sites on Hec1 at kinetochores are phosphorylated by Aurora kinase A rather
493 than Aurora kinase B[27,34,35] and other data indicating that Aurora kinase B can fulfill its mitotic
494 function without being targeted to centromeres in some systems[36]. Compared to Aurora kinase B,
495 relatively little is known about how Aurora kinase A regulates k-MT attachments, although
496 recent studies indicate that Aurora kinase A might also localize to kinetochores and
497 phosphorylate substrates there or regulate kinetochore substrates on chromosomes proximal to
498 the spindle pole[34,35]. Our data demonstrates that Aurora kinase A also regulates kinetochore
499 substrate phosphorylation indirectly through regulation of BOD1L1 as a negative regulator of
500 PP2A, and that this role for Aurora kinase A is responsible for changes in k-MT attachment
501 stability induced by prolonged increase in MCAK activity caused by UMK57 treatment. In this
502 context, an intriguing possibility emerges whereby the Aurora kinase A – BOD1L1 – PP2A axis
503 identified in this work is activated by hypostable k-MT attachments (or hypostable spindle MTs
504 more broadly) and induces a compensating increase in k-MT stability. Conversely, Aurora kinase
505 B has a well-recognized role in decreasing k-MT stability. Together, overall k-MT stability (and
506 perhaps total spindle MT stability and/or density) would be established through a lower bound
507 regulated by Aurora kinase A activity and an upper bound regulated by Aurora kinase B activity.
508 In support of this idea, TPX2 may serve as a sensor of MT stability to marshal Aurora kinase A
509 as needed because TPX2 has been shown to sense and influence the conformational state of
510 microtubules[37] while promoting MT assembly by suppressing tubulin subunit off-rates[38].
511 Moreover, this role for Aurora kinase A in stabilizing spindle microtubules through BOD1L1 is
512 consistent with many tumor cells overexpressing or having hyperactive Aurora kinase A[39–41] and
513 also being CIN as a consequence of hyperstable k-MT attachments. Our observations suggest
514 that depending on the context, Aurora kinase A may destabilize k-MT attachments through direct

515 kinetochore substrate phosphorylation or stabilize k-MT attachments through indirect regulation
516 of PP2A activity.

517 Importantly, we found that the gene encoding BOD1L1 is occasionally altered in human
518 cancers. Most of these alterations are point mutations, but some amplifications and deletions also
519 occur (Figure 8A). In uterine endometrial cancer, the cancer that most commonly has BOD1L1
520 alterations, the alterations are associated with a reduced likelihood of death. The functional
521 consequence of these mutations remains unknown, although it is likely that at least some of them
522 cause a loss of BOD1L1 function. Thus, a reduced likelihood of death would be consistent with
523 our findings that BOD1L1 knockdown results in a loss of fitness of various tumor lines and
524 vulnerability to taxol or Aurora kinase A inhibitor (Figure 8C, 8D), which is corroborated by the
525 mitotic arrest and occasional mitotic catastrophe observed in cells with BOD1L1 knockdown
526 even in the absence of these drugs (Figure 5E, S3A). Since BOD1L1 also plays an important role
527 in the cellular response to DNA replication stress and DNA repair[16,17], these alterations may also
528 contribute to the loss of cell fitness through that role. In contrast to patients with uterine
529 endometrial cancer, alterations in BOD1L1 were associated with an increased risk of death in
530 lung adenocarcinoma and in skin cutaneous skin melanoma. The clinically differing impacts of
531 BOD1L1 alteration might depend on whether it is the mitotic functions and/or DNA repair
532 functions that have been altered relative to the alterations at the root of a specific type of cancer.
533 For example, both lung adenocarcinoma (if caused by smoking) and skin melanoma are driven
534 by DNA damage caused by chemicals or UV light, thus possibly highlighting the role of
535 BOD1L1 in DNA repair. Whereas in endometrial cancer, the cyclic high proliferation rate of this
536 tissue in fertile women might highlight the role of BOD1L1 in maintaining accurate mitosis and
537 avoiding CIN.

538 In summary, this work defines a new regulatory pathway in cells including Aurora kinase
539 A, BOD1L1 and PP2A that is required for timely mitotic progression, faithful chromosome
540 segregation, and regulation of proper microtubule stability. Our data expand on the previously
541 known role for BOD1L1 as well as the previously known role of Aurora kinase A and provide
542 insight into cellular responses that lead to adaptation to a small molecule suppressor of the CIN
543 phenotype.
544

545 **Methods**

546 Cell Culture

547 SW620, HCT116, HeLa and U20S cells were obtained from the ATCC. HEC1 cells were a gift
548 from Tyler Curiel. All cells were grown at 37°C in a humidified environment with 5% CO_2.
549 SW620, HeLa and U2OS cell lines were grown in Dulbecco's modified Eagle medium
550 (Corning® #15-017-CM) containing 10% FCS (Hyclone #82013-586), 250µg/L Amphotericin B
551 (VWR #82026-728), 50 U/mL penicillin and 50 µg/mL streptomycin (ThermoFisher Scientific
552 #15140122). HCT116 and HEC1 cells were grown in McCoy's 5A medium with the same
553 supplements. Cells were verified to be free of mycoplasma by frequent staining of plated cells
554 with DAPI. No contamination was observed.

555 Inhibitors and reagents

556 The CENP-E inhibitor GSK-923295 (MedChemExpress LLC # HY-10299) was used at 200 nM.
557 NOC (VWR #80058-500) was used at 100-500 ng/ml. STLC (Tocris #2191) was used at 25 µM.
558 ProTAME (Concept Life Sciences custom synthesis) was used at 25 µM. Okadaic acid (LC Labs
559 O-5857) was used at 200 nM. RO-3306 (Selleck #S7747) was used at 10 µM. AZ3146 (R&D
560 Systems #3994/10) was used at 2µM. BI2536 (Synthesized in-house) was used at 100
561 nM. MLN8237 (Selleck #S1133) was used at 10-50 nM. ZM447439 (Tocris Bioscience
562 #2458/10) was used at 2 µM. UMK57 (Aobious #AOB8668) was used at 100 nM.

563 Plasmids and cloning

564 The pLKO.1 – TRC cloning vector was a gift from David Root (Addgene plasmid # 10878;
565 http://n2t.net/addgene:10878 ; RRID:Addgene_10878). The shRNA sequences were cloned into
566 the AgeI and EcoRI sites of the plasmid using standard cloning techniques. The DNA constructs
567 were then verified by Sanger sequencing and amplified by maxiprep (Qiagen #12162).

568 Lentiviruses were produced by co-transfection of 293T/17 cells with pVSV-G and pdVPR29.1
569 plasmids. 48 hours later, the virus containing supernatant was harvested, briefly centrifuged to
570 remove cell debris and frozen at -80ºC until further use.

571 Proteomic Screens

572 For the total protein and phospho-proteomic screen, ~80% confluent cells were re-plated at a
573 1:10 dilution on 15 cm plates. 3 dishes were treated with DMSO and 3 with UMK57. 72 hours
574 later, 2 dishes each of control and UMK57 treated cells were treated with 2.5 mM thymidine, and
575 continuing DMSO/UMK57 treatment. 24 hours following thymidine addition, it was washed out
576 with 2 washes of 5 ml PBS, and then fresh media added containing 100 ng/ml nocodazole, still
577 containing DMSO/UMK57. 16 hours later the DMSO treated cells were treated for 1 hour with
578 UMK57. The mitotic cells were harvested by shakeoff, centrifugation followed by a wash with 5
579 ml PBS, re-centrifugation and finally frozen at -80ºC before mass spectrometry analysis.
580 Separately, following the 72 hours DMSO/UMK57 treatment, the remaining dishes were
581 trypsinized and re-plated on glass coverslips for microscopy analysis.

582 Sample preparation: Samples were prepared essentially as previously described[42,43], with a few
583 modifications. Cells were lysed in 8M urea, 200 mM EPPS, pH 8.5, supplemented with 1X
584 Pierce protease and phosphatase inhibitors. The resuspended samples were passed through a 1.5-
585 inch 21-gauge needle to ensure DNA were sheared. Protein concentration was determined for
586 each sample with BCA. Samples were reduced with 5 mM TCEP at room temperature for 20
587 min, alkylated with 10 mM iodoacetamide at room temperature for 20 min in the dark, and then
588 quenched with 10 mM DTT at room temperature for 20 min in the dark. Methanol-chloroform
589 precipitation was performed prior to protease digestion. In brief, 4-parts neat methanol were
590 added to each sample and vortexed, 1-part chloroform was added to the sample and vortexed,

591 and 3-parts water was added to the sample and vortexed. The sample was centrifuged at 14,000
592 RPM for 2 min at room temperature and subsequently washed once with 100% methanol.
593 Samples were resuspended in 200 mM EPPS, pH 8.5 and digested at room temperature for 14 h
594 with Lys-C protease at a 50:1 protein-to-protease ratio. Trypsin was then added at a 100:1
595 protein-to-protease ratio and the reaction was incubated for 6 h at 37°C.
596 Fe^{3}+-NTA phosphopeptide enrichment: Following digestion with Lys-C and trypsin, peptides
597 were desalted by using 100mg SepPak columns. The elutions were dried via vacuum
598 centrifugation and the phosphopeptides were enriched with the High-Select Fe3+-NTA
599 Phosphopeptide Enrichment Kit according to manufacturer's specifications using approximately
600 4 mg protein digest per enrichment column. The elutions were dried via vacuum centrifugation,
601 while the flow-throughs were saved for subsequent whole proteome analysis.
602 TMT labeling: In general, we estimate that at most 20 ug of phosphopeptides were enriched from
603 4 mg of total peptide. We added 40 ug of TMT 6-plex reagent (Thermo-Fisher) to the peptides
604 along with acetonitrile to again achieve a final acetonitrile concentration of approximately 30%
605 (v/v) in a total volume of 50 µL. Following incubation at room temperature for 1 h, the reaction
606 was quenched with hydroxylamine to a final concentration of 0.3% (v/v). The sample was
607 vacuum centrifuged to near dryness and subjected to C18 solid-phase extraction (SPE, Sep-Pak).
608 Off-line basic pH reversed-phase (BPRP) fractionation: We fractionated the peptide samples
609 using BPRP HPLC. We used an Agilent 1200 pump equipped with a degasser and a UV detector.
610 Peptides were subjected to a 50-min linear gradient from 5% to 35% acetonitrile in 10 mM
611 ammonium bicarbonate pH 8 at a flow rate of 0.6 mL/min over an Agilent 300Extend C18
612 column (3.5 µm particles, 4.6 mm ID and 250 mm in length). The peptide mixture was
613 fractionated into a total of 96 fractions, which were consolidated into 12 super-fractions.

614 Samples were subsequently acidified with 1% formic acid and vacuum centrifuged to near
615 dryness. Each consolidated fraction was desalted by StageTip, and reconstituted in 5%
616 acetonitrile, 5% formic acid for LC-MS/MS processing.
617 Liquid chromatography and tandem mass spectrometry: Mass spectrometric data were collected
618 on an Orbitrap Lumos mass spectrometer coupled to a Proxeon NanoLC-1200 UHPLC
619 (ThermoFisher Scientific). The 100 µm capillary column was packed in-house with 35 cm of
620 Accucore 150 resin (2.6 µm, 150Å; ThermoFisher Scientific). Data were acquired for 180 min
621 per fraction. MS1 spectra were acquired at 120 K resolving power for a maximum of 50 ms in
622 the Orbitrap, and features were filtered for monoisotopic peak assignment and charge states 2-6.
623 MS2 spectra were acquired by selecting the top 10 most abundant features. MS2 spectra were
624 acquired via collisional induced dissociation (CID), in the ion trap with an automatic gain control
625 (AGC) of 20K, quadrupole isolation width of 0.5 m/z and a maximum ion time of 120 ms with
626 Multistage Activation turned on. For MS3 acquisition, a synchronous precursor selection (SPS)
627 of 10 fragments ions was acquired for a maximum of 150 ms with an AGC of 300K and a
628 normalized collision energy of 65.
629 Data analysis: Database searching included all entries from the mouse UniProt Database
630 (downloaded: 2014). The database was concatenated with one composed of all protein sequences
631 for that database in the reversed order[44]. Raw files were converted to mzXML, and monoisotopic
632 peaks were re-assigned using Monocle[45]. Searches were performed with SEQUEST[46] using a 20-
633 ppm precursor ion tolerance. TMT labels on lysine residues and peptide N-termini (+229.1629
634 Da), as well as carbamidomethylation of cysteine residues (+57.021 Da) were set as static
635 modifications, while oxidation of methionine residues (+15.995 Da) and phosphorylation
636 (+79.966) were set as variable modifications. Peptide-spectrum matches (PSMs) were adjusted to

637 a 1% false discovery rate (FDR) using a linear discriminant after which proteins were assembled
638 further to a final protein-level FDR of 1% analysis[47]. Ascore was used to determine site
639 localization[48], with a score of 13 denoting 95% confidence for a specified phosphorylation site.
640 Phosphorylation sites were quantified by summing reporter ion counts across all matching PSMs.
641 Peptides were filtered to include only those with a summed signal-to-noise (SN) ≥ 100 across all
642 TMT channels as well as an isolation specificity ("isolation purity") of at least 0.5.

643 Whole Proteome Profiling

644 Sample preparation for whole proteome profiling: Flow-throughs from the phospho-enrichment
645 described above, 50 µg per replicate, were used for the whole proteome work for each sample.
646 TMT labeling: 120 µg of TMTpro reagents (Thermo-Fisher; Lot # WL338745) were added to
647 the peptides (50 µg) along with acetonitrile to achieve a final acetonitrile concentration of
648 approximately 30% (v/v) in a total volume of 100 µL. Following incubation at room temperature
649 for 1 h, the reaction was quenched with hydroxylamine to a final concentration of 0.3% (v/v).
650 The sample was vacuum centrifuged to near dryness and subjected to C18 solid-phase extraction
651 (SPE, Sep-Pak).
652 Off-line basic pH reversed-phase (BPRP) fractionation: We fractionated the peptide samples
653 using BPRP HPLC. We used an Agilent 1200 pump equipped with a degasser and a UV detector.
654 Peptides were subjected to a 50-min linear gradient from 5% to 35% acetonitrile in 10 mM
655 ammonium bicarbonate pH 8 at a flow rate of 0.6 mL/min over an Agilent 300Extend C18
656 column (3.5 µm particles, 4.6 mm ID and 250 mm in length). The peptide mixture was
657 fractionated into a total of 96 fractions, which were consolidated into 24 super-fractions (in a
658 checkerboard-like pattern) of which 12 were used for data acquisition. Samples were
659 subsequently acidified with 1% formic acid and vacuum centrifuged to near dryness. Each

660 consolidated fraction was desalted by StageTip, and reconstituted in 5% acetonitrile, 5% formic
661 acid for LC-MS/MS processing.
662 Liquid chromatography and tandem mass spectrometry. Mass spectrometric data were collected
663 on an Orbitrap Fusion mass spectrometer coupled to a Proxeon NanoLC-1200 UHPLC
664 (ThermoFisher Scientific). A 100 µm capillary column was packed in-house with 35 cm of
665 Accucore 150 resin (2.6 µm, 150Å; ThermoFisher Scientific). Data were acquired for 180 min
666 per fraction. MS1 spectra were acquired at 120 K resolving power for a maximum of 100 ms in
667 the Orbitrap, and features were filtered for monoisotopic peak assignment and charge state of 2.
668 MS2 spectra were acquired by selecting the top 10 most abundant features. MS2 spectra were
669 acquired via collisional induced dissociation (CID), in the ion trap with an automatic gain control
670 (AGC) of 9K, quadrupole isolation width of 0.7 m/z at Rapid Scan Rate. For MS3 acquisition, a
671 synchronous precursor selection (SPS) of 10 fragments ions was acquired for a maximum of 200
672 ms with an AGC of 200K and a normalized collision energy of 55.
673 Data analysis. Searches were performed as described above but without phosphorylation variable
674 modifications. Proteins were quantified by summing reporter ion counts across all matching
675 PSMs. More specifically, reporter ion intensities were adjusted to correct for the isotopic
676 impurities of the different TMTpro reagents according to manufacturer specifications. Peptides
677 were filtered to include only those with a summed signal-to-noise (SN) ≥ 100 across all TMT
678 channels and isolation specificity of at least 0.5. The signal-to-noise (S/N) measurements of
679 peptides assigned to each protein were summed (for a given protein) and each protein abundance
680 measurement was scaled, such that the summed signal-to-noise for that protein across all
681 channels equals 100, thereby generating a relative abundance (RA) measurement.
682 <u>Transfections</u>

683 200,000 SW620 cells were plated on glass coverslips in 12-well plates. 24 hours following
684 plating, they were transfected with 1 μg plasmid DNA and 2.5 μl Lipofectamine™ 2000
685 (ThermoFisher #11668027) in a total of 1 ml Opti-MEM™ media (ThermoFisher #31985070).
686 Four hours following transfection, the media was changed for DMEM containing 2μg/ml
687 puromycin. The cells were then assayed 48-72 hours following addition of puromycin.
688 SDS-PAGE and Western blot
689 Gels and blots were performed as described previously [49]. Prior to loading samples on gel, 4X
690 Laemmli buffer (200 mM Tris pH 6.8, 4% SDS, 40% glycerol, 4% 2-mercaptoethanol, 0.12
691 mg/ml bromophenol blue) was added to a final dilution of 1X, and the samples were boiled for 5
692 minutes. Proteins were separated on SDS-PAGE gel using stacking gel (4% 29:1 acrylamide:
693 Bis-acrylamide, 125mM Tris pH 6.8, 0.1% SDS, 0.1% ammonium persulfate, 0.1% TEMED)
694 and (8-15% 29:1 acrylamide: Bis-acrylamide, 400 mM Tris pH 8.8, 0.1% SDS, 0.1% ammonium
695 persulfate, 0.1% TEMED) at 120V until the bromophenol blue has run off or longer, as needed.
696 Transfer onto nitrocellulose membrane was performed for at least 24 hours at 30V under wet
697 conditions in 1X transfer buffer (14.4 g/L glycine, 3.0 g/L Tris, 20% methanol). Conditions for
698 western blots includes the use of 5% nonfat dry milk in TBS-T 0.5% (50 mM Tris [pH 7.2], 150
699 mM NaCl, 0.5% Tween 20) for blocking and TBS-T 0.5% for washing. 4 washes for 10 minutes
700 each were performed after primary and secondary antibody incubation periods. The bands were
701 visualized by enhanced chemiluminescence using Clarity (Bio-Rad #1705060) using a Bio-Rad
702 ChemiDoc MP.
703 Immunoprecipitation
704 Protein-G beads were first crosslinked to the antibody by incubating the beads and antibody
705 overnight on a rotating platform. The beads were then washed with PBS and then crosslinking

706 solution (20mM dimethyl pimelimidate, 0.3M HEPES in ice cold water). The beads were then
707 incubated in crosslink solution for 10 minutes at room temperature. The solution is then
708 discarded, and the incubation repeated in fresh crosslink buffer, which is performed three times.
709 The beads are then washed in PBS twice and twice with lysis buffer prior to use.
710 SW620 cells from confluent 15 cm dishes were split 1:5. 48 hours later, 2.5 mM thymidine was
711 added. 24 hours following thymidine addition, it was washed out with 2 5ml washes with PBS.
712 Fresh media containing 100 ng/ml nocodazole was then added. 16 hours later, the cells were
713 harvested by scraping, washed once with cold PBS, and lysed in the following buffer: 0.5%
714 NP40, 100 mM NaCl, 50 mM tris pH 7.4, 10 mM glycerol 2-phosphate. Cells were lysed on ice
715 for 20 minutes before centrifuging at 15,000 x g for 20 minutes at 4ºC. The supernatant was
716 transferred to a fresh tube, and input sample set aside. 10 µl of packed volume protein G beads
717 cross-linked to antibody were added to each sample for 2 hours on a rotating platform at 4ºC.
718 The beads were then washed 5 times in lysis buffer and dried using a 30 g needle attached to a
719 vacuum line. 30-100 µl of 1X sample buffer were added to the beads before elution by boiling
720 and loading on gel.
721 Identification of BOD1L1 interacting proteins
722 Excised gel bands were cut into approximately 1 mm^3 pieces. Gel pieces were then subjected to a
723 modified in-gel trypsin digestion procedure[50]. Gel pieces were washed and dehydrated with
724 acetonitrile for 10 min. followed by removal of acetonitrile. Pieces were then completely dried in
725 a speed-vac. Rehydration of the gel pieces was with 50 mM ammonium bicarbonate solution
726 containing 12.5 ng/µl modified sequencing-grade trypsin (Promega, Madison, WI) at 4ºC. After
727 45 min., the excess trypsin solution was removed and replaced with 50 mM ammonium
728 bicarbonate solution to just cover the gel pieces. Samples were then placed in a 37ºC room

729 overnight. Peptides were later extracted by removing the ammonium bicarbonate solution,
730 followed by one wash with a solution containing 50% acetonitrile and 1% formic acid. The
731 extracts were then dried in a speed-vac (~1 hr). The samples were then stored at 4ºC until
732 analysis. On the day of analysis the samples were reconstituted in 5 – 10 µl of HPLC solvent A
733 (2.5% acetonitrile, 0.1% formic acid). A nano-scale reverse-phase HPLC capillary column was
734 created by packing 2.6 µm C18 spherical silica beads into a fused silica capillary (100 µm inner
735 diameter x ~30 cm length) with a flame-drawn tip[51]. After equilibrating the column each sample
736 was loaded via a Famos auto sampler (LC Packings, San Francisco CA) onto the column. A
737 gradient was formed and peptides were eluted with increasing concentrations of solvent B
738 (97.5% acetonitrile, 0.1% formic acid). As peptides eluted they were subjected to electrospray
739 ionization and then entered into an LTQ Orbitrap Velos Pro ion-trap mass spectrometer (Thermo
740 Fisher Scientific, Waltham, MA). Peptides were detected, isolated, and fragmented to produce a
741 tandem mass spectrum of specific fragment ions for each peptide. Peptide sequences (and hence
742 protein identity) were determined by matching protein databases with the acquired fragmentation
743 pattern by the software program, Sequest (Thermo Fisher Scientific, Waltham, MA)[46]. All
744 databases include a reversed version of all the sequences and the data was filtered to between a
745 one and two percent peptide false discovery rate.

746 GST pulldowns

747 We performed GST-pulldowns essentially as described previously[17]. Briefly, SW620 mitotic
748 nuclear extracts were incubated with 1 µg of GST-fusion protein or purified GST as a control on
749 a rotating platform for 3 hours. Bound proteins were then purified via binding to glutathione
750 Sepharose (GE Healthcare) and washed. Samples were then analyzed by Western blot.

751 RNA interference

752 Gene knockdown was performed by cloning the following shRNA sequences into the PLKO1
753 vector and then transfecting cells with 1μg of plasmid DNA and 2.5μl lipofectamine 2000 per ml
754 according to the manufacturer's directions. Media was changed after 5 hours, and puromycin
755 added after 24 hours.
756 BOD1L1-1: 5'- GCCAATGATGCCATGTCGATA-3'
757 BOD1L1-2: 5'- ACTCGCATGTATCCAAGTAAA-3'
758 Immunofluorescence
759 Following treatments, cells were pre-extracted in PHEM buffer (60 mM PIPES, 25 mM HEPES,
760 pH 6.9, 10 mM EGTA, and 4 mM $MgSO_4$, 1% Triton X-100, 10 mM glycerol 2-phosphate) for
761 10 minutes at 4ºC and then fixed in 4% paraformaldehyde in PBs at room temperature for 20
762 minutes. The remaining steps were performed at room temperature. The cells were then washed
763 twice with PBS for before blocking with ADB (10% serum, 0.1% Triton X-100 in PBS) for 15
764 minutes. Primary antibodies were then diluted in ADB and used at the indicated dilution.
765 Secondary antibodies were diluted in ADB. After incubation with antibodies, the cells were
766 washed three times with PBS 0.1% Triton X-100. Finally, the cells were counterstained with
767 DAPI and mounted on slides using ProLong™ Gold antifade reagent (ThermoFisher Scientific
768 #P36934).
769 Microscopy
770 Images were acquired with a Nikon Eclipse Ti microscope equipped with a cooled charge-
771 coupled device Clara camera (Andor Technology) controlled by Nikon NIS-Elements software
772 version 4.30.02. Images were acquired in 0.15-0.4 μm sections using a plan apo 1.4 numerical
773 aperture 100X (kinetochore analysis) or 60X (lagging chromosome analysis) oil-immersion
774 objective using 1X1 binning. Samples were illuminated using an X-cite light source (Excelitas

775 Technologies Corp). All image analysis, adjustment and cropping was performed using Fiji
776 software [52]. Image deconvolution was performed using Nikon Elements batch deconvolution
777 software version 5.21.00 on automatic mode. All kinetochore intensity analysis was performed
778 on the raw images, except for microtubule intensity determination for which deconvolution was
779 performed prior to analysis. Line scans were performed on the deconvoluted images in Fiji and
780 the data was then exported to Graphpad Prism. All images of BOD1L1 selected for presentation
781 are deconvolved single optical slices. Images of other stained proteins are deconvolved
782 maximum intensity projections. Where shown, insets are from single optical Z-slices. Images
783 were selected to represent the mean quantified data. Quantification of kinetochore staining
784 intensity was performed by first determining the brightest plane for which a given kinetochore
785 appears. Then, an outline was drawn using the ellipse tool. The integrated intensity was
786 determined by multiplying the average intensity by the area of the kinetochore. Background
787 levels of staining were determined by saturating the brightness and contrast settings to find the
788 darkest spot within the chromatin containing area and were subtracted from the intensity of the
789 kinetochore. Aurora kinase A pT288 was quantified by first creating a sum projection of the
790 image. Then, an outline was drawn around the whole cell, and the fluorescence intensity
791 measured. The background-subtracted, normalized integrated intensities for all cells were then
792 plotted. To quantify levels of cold-stable microtubules, images were first deconvolved. Then, A
793 sum-intensity projection was created in Fiji. Viewing the ACA channel, a rectangle was drawn
794 that was 2 μm wide in the pole-pole axis, and as long as the furthest centromeres in the
795 metaphase plate. Then, switching to the tubulin channel, the average tubulin intensity was
796 measured in the rectangle. From the average intensity value, the minimum intensity value was
797 used as the background level and subtracted. The Background-subtracted intensity values were

798 then averaged across all of the cells that were analyzed for each condition and experimental
799 repeat.
800 For live-cell microscopy, cells were transfected with 0.5 μg of mCherry-H2B-expressing plasmid
801 together with pLKO vectors. After selection with puromycin, the cells were washed twice with
802 PBS, given fresh medium and moved to a Tokai Hit incubation chamber with CO_2 and
803 temperature control on the microscope. The cells were imaged every 5 minutes at 20X
804 magnification for 48 hours with 2X2 binning.
805 Antibodies
806 The following antibodies were used for immunofluorescence (IF) and/or immunoblotting (IB):
807 human anti-ACA (Geisel School of Medicine; IF at 1:2000), mouse anti-Hec1 (Santa Cruz C-11;
808 IF,IB at 1:1000), mouse anti-PP2AR1A (Santa Cruz SC-74580; IB at 1:500), mouse anti-
809 PP2AC (Santa Cruz SC-166034; IB at 1:500), rabbit anti-PP2A B56 Alpha
810 (MyBioSource.com MBS8524809; IB at 1:500), mouse anti-PP2A B56 Beta (Santa Cruz E-6; IB
811 at 1:500), mouse anti-PP2A B56 Gamma (Santa Cruz A-11; IB at 1:500), mouse anti-PP2A B56
812 Delta (Santa Cruz H-11; IB at 1:500), rabbit anti-PP2A B56 Epsilon (Aviva Systems Biology
813 RP56694_P050; IB at 1:500), rabbit anti-Hec1 pS44 (gift of Jennifer DeLuca; IF at 1:500)[53],
814 rabbit anti DSN1 pS100 (gift of Iain Cheeseman; IF at 1:250)[54], rabbit anti-KNL1 pT943/pT1155
815 (Cell Signaling #40758), mouse anti-α-Tubulin DM1α (Sigma-Aldrich; IF at 1:4000-1:10,000),
816 mouse anti-Aurora A (Cell Signaling Technology 1F8; IF at1:1000), Rabbit anti-Aurora A
817 pT288 (Cell Signaling Technology C39D8; IF at 1:500), Rabbit anti-TACC3 (gift of Jordan
818 Raff; IF at 1:1000)[55], mouse anti-TPX2 (Cell Signaling Technology D9Y1V; IF at 1:1000),
819 rabbit anti-Aurora B pT232 (Rockland 600-401-677; IF/IB at 1:1000), rabbit anti-MCAK pS95
820 (Abcam #AB74146; IF/IB at 1:500), rabbit anti-Hec1 pT31[26] (IF at 1:100,000, WB at 1:1000),

821 rabbit anti-BOD1L1 (IF at 1:1000) (gift of Grant Stewart[16]), rabbit anti-BOD1L1 (Genetex
822 #GTX119946; WB at 1:500). Secondary antibodies used were highly cross-adsorbed Alexa
823 Fluor® 488, 594 and 647 raised in donkey or goat (Invitrogen; IF at 1:1000), horseradish
824 peroxidase (Bio-Rad; IB at 1:10000-10,0000), Mouse TrueBlot® ULTRA: rat Anti-Mouse IgG
825 (Rockland 18-8817-33; IB at 1:1000), Anti-IgG (H+L) Goat Polyclonal Antibody (Horseradish
826 Peroxidase), Peroxidase AffiniPure Goat Anti-Rabbit IgG (H+L) (IB at 1:5000), Goat Polyclonal
827 Antibody (Horseradish Peroxidase), Peroxidase AffiniPure Goat Anti-Mouse IgG (H+L) (IB at
828 1:5000).

829 Statistical analysis of cell biology data

830 All statistical tests were performed using Graphpad Prism version 8.4.2. Except where indicated,
831 all experiments were performed as 2-3 independent biological repeats. In most IF experiments,
832 20 cells per repeat were analyzed, and 25 kinetochores for each cell measured. Experiments with
833 other numbers are noted in the figure legends. For anaphase error rates, 100 anaphases per
834 condition were assessed for each of 3 independent biological experiments. Statistical significance
835 was calculated between indicated conditions using two-tailed *t*-tests or Dunnett's multiple
836 comparison test. For these tests, the data distribution was assumed to be normal but this was not
837 formally tested.

838 Study population data, and statistical analysis

839 The cBioPortal for Cancer Genomics was used to query and visualize *BOD1L1* alterations in
840 data from The Cancer Genome Atlas (TCGA). Then, TCGA PanCancer Atlas cancer specific
841 clinical and *BOD1L1* alteration data was downloaded via cBioPortal for Cancer Genomics for
842 cancer types where *BOD1L1* alteration was most frequent: uterine corpus endometrial carcinoma
843 TCGA-UCEC PCA (n= 529), lung adenocarcinoma TCGA-LUAD (n = 667), cutaneous

844 melanoma TCGA-SKCM (n = 448), stomach adenocarcinoma TCGA-STAD (n = 440), and lung
845 squamous cell carcinoma TCGA-LUSC (n = 487). All statistical analysis was conducted in R
846 version 4.2.1. Survival analysis using Kaplan-Meier plots and Cox Proportional-Hazards models
847 was conducted using R package *survival* and plotted using R package *survminer*. Univariate
848 Kaplan-Meier survival strata were plotted for altered *BOD1L1* status in each cancer type to
849 assess five-year overall survival status. Cox Proportional Hazards models for each cancer type
850 tested association of *BOD1L1* alteration status with adjustment for patient age, sex (excepting
851 uterine), and tumor stage or grade. Using Fisher's exact tests and patient data from all TCGA-
852 PanCancer Atlas cancer datasets (n = 10,967 from 32 cancer types), we tested whether *BOD1L1*
853 alterations were exclusive of alterations to other Aurora A-BOD1L1- PP2A gene pathway
854 members.

855 Data availability

856 The cell biology datasets generated during and/or analysed during the current study are available
857 from the corresponding author on reasonable request. The MS datasets will be uploaded to an
858 appropriate public repository upon acceptance of the article.

859

Acknowledgements

We thank Grant Stewart, Jennifer Delucca, Iain Cheeseman, Tyler Curiel, Jose Teodoro and Adrian Saurin for providing reagents. We also thank Sanjukta Guha Thakurta (Thermo Fisher Center for multiplexed proteomics, Harvard University) and Ross Tomaino (Taplin Mass Spectrometry Facility, Harvard University) for assistance with the proteomics analysis. We also thank the members of the Compton laboratory for helpful discussions and feedback. TJK was supported by fellowships from the Fonds de Recherche du Québec – Santé and the Canadian Institutes of Health Research. The laboratory of SB is supported by grants from the Canadian Institutes of Health Research (PJT-156193) and Natural Sciences and Engineering Research Council of Canada (NSERC; RGPIN-2017-04649). This work was also supported by grants from the National Institutes of Health #GM051542 to DAC. The authors acknowledge the following Shared Resources facilities (Bio-Rad ChemiDoc MP) at the Norris Cotton Cancer Center at Dartmouth with NCI Cancer Center Support Grant 5P30 CA023108-40.

Author Contributions

Conceptualization: DAC and TJK. Investigation: TJK, IMV, MRH. Formal analysis: TJK, IMV. Methodology: TJK, DAC. Funding acquisition: TJK, DAC. Supervision: BCC, SB, DAC. Writing- original draft: TJK. Writing- review & editing: TJK, MRH, BCC, DAC. Project administration: DAC.

Competing interests

The authors declare that they have no conflicts of interest

Materials & Correspondence

Any requests should be addressed to DAC

883 **References**

884 1. Luo, J., Solimini, N. L. & Elledge, S. J. Principles of Cancer Therapy: Oncogene and Non-
885 oncogene Addiction. *Cell* **136**, 823–837 (2009).
886 2. Geigl, J. B., Obenauf, A. C., Schwarzbraun, T. & Speicher, M. R. Defining 'chromosomal
887 instability'. *Trends Genet.* **24**, 64–69 (2008).
888 3. Lengauer, C., Kinzler, K. W. & Vogelstein, B. Genetic instability in colorectal cancers.
889 *Nature* **386**, 623–627 (1997).
890 4. Thompson, S. L. & Compton, D. A. Chromosome missegregation in human cells arises
891 through specific types of kinetochore-microtubule attachment errors. *Proc. Natl. Acad. Sci.*
892 **108**, 17974–17978 (2011).
893 5. Bakhoum, S. F., Thompson, S. L., Manning, A. L. & Compton, D. A. Genome stability is
894 ensured by temporal control of kinetochore–microtubule dynamics. *Nat. Cell Biol.* **11**, 27–35
895 (2009).
896 6. Kleyman, M., Kabeche, L. & Compton, D. A. STAG2 promotes error correction in mitosis by
897 regulating kinetochore-microtubule attachments. *J. Cell Sci.* jcs.151613 (2014)
898 doi:10.1242/jcs.151613.
899 7. Bakhoum, S. F., Genovese, G. & Compton, D. A. Deviant Kinetochore Microtubule
900 Dynamics Underlie Chromosomal Instability. *Curr. Biol.* **19**, 1937–1942 (2009).
901 8. Bakhoum, S. F., Kabeche, L., Murnane, J. P., Zaki, B. I. & Compton, D. A. DNA-Damage
902 Response during Mitosis Induces Whole-Chromosome Missegregation. *Cancer Discov.* **4**,
903 1281–1289 (2014).
904 9. Hunter, A. W. *et al.* The Kinesin-Related Protein MCAK Is a Microtubule Depolymerase that
905 Forms an ATP-Hydrolyzing Complex at Microtubule Ends. *Mol. Cell* **11**, 445–457 (2003).

906 10. Maney, T., Hunter, A. W., Wagenbach, M. & Wordeman, L. Mitotic Centromere–
907 associated Kinesin Is Important for Anaphase Chromosome Segregation. *J. Cell Biol.* **142**,
908 787–801 (1998).
909 11. Orr, B., Talje, L., Liu, Z., Kwok, B. H. & Compton, D. A. Adaptive Resistance to an
910 Inhibitor of Chromosomal Instability in Human Cancer Cells. *Cell Rep.* **17**, 1755–1763
911 (2016).
912 12. Huang, H. *et al.* Tripin/hSgo2 recruits MCAK to the inner centromere to correct defective
913 kinetochore attachments. *J. Cell Biol.* **177**, 413–424 (2007).
914 13. Tanno, Y. *et al.* Phosphorylation of mammalian Sgo2 by Aurora B recruits PP2A and
915 MCAK to centromeres. *Genes Dev.* **24**, 2169–2179 (2010).
916 14. Kettenbach, A. N. *et al.* Quantitative Phosphoproteomics Identifies Substrates and
917 Functional Modules of Aurora and Polo-Like Kinase Activities in Mitotic Cells. *Sci. Signal.* **4**,
918 rs5–rs5 (2011).
919 15. Arslanhan, M. D., Rauniyar, N., Yates, J. R. & Firat-Karalar, E. N. Aurora Kinase A
920 proximity map reveals centriolar satellites as regulators of its ciliary function. *EMBO Rep.* **22**,
921 (2021).
922 16. Higgs, M. R. *et al.* BOD1L Is Required to Suppress Deleterious Resection of Stressed
923 Replication Forks. *Mol. Cell* **59**, 462–477 (2015).
924 17. Bayley, R. *et al.* H3K4 methylation by SETD1A/BOD1L facilitates RIF1-dependent
925 NHEJ. *Mol. Cell* **82**, 1924-1939.e10 (2022).
926 18. Moustafa-Kamal, M., Gamache, I., Lu, Y., Li, S. & Teodoro, J. G. BimEL is
927 phosphorylated at mitosis by Aurora A and targeted for degradation by βTrCP1. *Cell Death*
928 *Differ.* **20**, 1393–1403 (2013).

929 19. Kufer, T. A. *et al.* Human TPX2 is required for targeting Aurora-A kinase to the spindle.
930 *J. Cell Biol.* **158**, 617–623 (2002).
931 20. Higgs, M. R. *et al.* Histone Methylation by SETD1A Protects Nascent DNA through the
932 Nucleosome Chaperone Activity of FANCD2. *Mol. Cell* **71**, 25-41.e6 (2018).
933 21. Porter, I. M. *et al.* Bod1, a novel kinetochore protein required for chromosome
934 biorientation. *J. Cell Biol.* **179**, 187–197 (2007).
935 22. Porter, I. M., Schleicher, K., Porter, M. & Swedlow, J. R. Bod1 regulates protein
936 phosphatase 2A at mitotic kinetochores. *Nat. Commun.* **4**, 2677 (2013).
937 23. Schleicher, K., Porter, M., Sundaramoorthy, R., Porter, I. M. & Swedlow, J. R. The
938 Ndc80 complex targets Bod1 to human mitotic kinetochores. 14.
939 24. Kazyken, D. *et al.* AMPK directly activates mTORC2 to promote cell survival during
940 acute energetic stress. *Sci. Signal.* **12**, eaav3249 (2019).
941 25. McKinley, K. L. & Cheeseman, I. M. Large-Scale Analysis of CRISPR/Cas9 Cell-Cycle
942 Knockouts Reveals the Diversity of p53-Dependent Responses to Cell-Cycle Defects. *Dev.*
943 *Cell* **40**, 405-420.e2 (2017).
944 26. Kucharski, T. J. Chromosome segregation fidelity is controlled by small changes in
945 phospho-occupancy at the kinetochore-microtubule interface. *J. Cell Biol.* (2022).
946 27. Sobajima, T. *et al.* PP6 regulation of Aurora A–TPX2 limits NDC80 phosphorylation and
947 mitotic spindle size. *J. Cell Biol.* **222**, e202205117 (2023).
948 28. Zaytsev, A. V. *et al.* Multisite phosphorylation of the NDC80 complex gradually tunes its
949 microtubule-binding affinity. *Mol. Biol. Cell* **26**, 1829–1844 (2015).
950 29. Herman, J. A. *et al.* Hyper-active RAS/MAPK introduces cancer-specific mitotic
951 vulnerabilities. *Proc. Natl. Acad. Sci.* **119**, e2208255119 (2022).

952 30. Meyers, R. M. *et al.* Computational correction of copy-number effect improves
953 specificity of CRISPR-Cas9 essentiality screens in cancer cells. (2018).
954 31. Joshua M. Dempster *et al.* Extracting Biological Insights from the Project Achilles
955 Genome-Scale CRISPR Screens in Cancer Cell Lines. *bioRxiv* 720243 (2019)
956 doi:10.1101/720243.
957 32. Nagelli, S. & Westermarck, J. CIP2A coordinates phosphosignaling, mitosis, and the
958 DNA damage response. *Trends Cancer* **10**, 52–64 (2024).
959 33. Pavic, K. *et al.* Structural mechanism for inhibition of PP2A-B56α and oncogenicity by
960 CIP2A. *Nat. Commun.* **14**, 1143 (2023).
961 34. DeLuca, K. F. *et al.* Aurora A kinase phosphorylates Hec1 to regulate metaphase
962 kinetochore–microtubule dynamics. *J. Cell Biol.* **217**, 163–177 (2018).
963 35. Ye, A. A. *et al.* Aurora A Kinase Contributes to a Pole-Based Error Correction Pathway.
964 *Curr. Biol.* **25**, 1842–1851 (2015).
965 36. Campbell, C. S. & Desai, A. Tension sensing by Aurora B kinase is independent of
966 survivin-based centromere localization. *Nature* **497**, 118–121 (2013).
967 37. Zhang, R., Roostalu, J., Surrey, T. & Nogales, E. Structural insight into TPX2-stimulated
968 microtubule assembly. *eLife* **6**, e30959 (2017).
969 38. Reid, T. A. *et al.* Suppression of microtubule assembly kinetics by the mitotic protein
970 TPX2. *J. Cell Sci.* jcs.178806 (2016) doi:10.1242/jcs.178806.
971 39. Bischoff, J. R. A homologue of Drosophila aurora kinase is oncogenic and amplified in
972 human colorectal cancers. *EMBO J.* **17**, 3052–3065 (1998).
973 40. Zhou, H. *et al.* Tumour amplified kinase STK15/BTAK induces centrosome
974 amplification, aneuploidy and transformation. *Nat. Genet.* **20**, 189–193 (1998).

975 41. Sen, S., Zhou, H. & White, R. A. A putative serine/threonine kinase encoding gene
976 BTAK on chromosome 20q13 is ampli®ed and overexpressed in human breast cancer cell
977 lines.
978 42. Navarrete-Perea, J., Yu, Q., Gygi, S. P. & Paulo, J. A. Streamlined Tandem Mass Tag
979 (SL-TMT) Protocol: An Efficient Strategy for Quantitative (Phospho)proteome Profiling
980 Using Tandem Mass Tag-Synchronous Precursor Selection-MS3. *J Proteome Res* (2018).
981 43. Li, J. *et al.* TMTpro-18plex: The Expanded and Complete Set of TMTpro Reagents for
982 Sample Multiplexing. *J Proteome Res* (2021).
983 44. Elias, J. E. & Gygi, S. P. Target-decoy search strategy for increased confidence in large-
984 scale protein identifications by mass spectrometry. *Nat. Methods* **4**, 207–214 (2007).
985 45. Rad, R. *et al.* Improved Monoisotopic Mass Estimation for Deeper Proteome Coverage. *J*
986 *Proteome Res* (2021).
987 46. Yates, J. R. An approach to correlate tandem mass spectral data of peptides with amino
988 acid sequences in a protein database.
989 47. Huttlin, E. L. A Tissue-Specific Atlas of Mouse Protein Phosphorylation and Expression.
990 48. Beausoleil, S. A., Villen, J., Gerber, S. A., Rush, J. & Gygi, S. P. A probability-based
991 approach for high-throughput protein phosphorylation analysis and site localization. *Nat.*
992 *Biotechnol.* **24**, (2006).
993 49. Kucharski, T. J., Minshall, P. E., Moustafa-Kamal, M., Turnell, A. S. & Teodoro, J. G.
994 Reciprocal Regulation between 53BP1 and the Anaphase-Promoting Complex/Cyclosome Is
995 Required for Genomic Stability during Mitotic Stress. *Cell Rep.* **18**, 1982–1995 (2017).
996 50. Shevchenko, A., Wilm, M., Vorm, O. & Mann, M. Mass Spectrometric Sequencing of
997 Proteins from Silver-Stained Polyacrylamide Gels. *Anal. Chem.* **68**, 850–858 (1996).

998 51. Peng, J. & Gygi, S. P. Proteomics: the move to mixtures. *J. Mass Spectrom.* **36**, 1083–
999 1091 (2001).
1000 52. Schindelin, J. *et al.* Fiji: an open-source platform for biological-image analysis. *Nat.*
1001 *Methods* **9**, 676–682 (2012).
1002 53. DeLuca, K. F., Lens, S. M. A. & DeLuca, J. G. Temporal changes in Hec1
1003 phosphorylation control kinetochore-microtubule attachment stability during mitosis. *J. Cell*
1004 *Sci.* **124**, 622–634 (2011).
1005 54. Welburn, J. P. I. *et al.* Aurora B Phosphorylates Spatially Distinct Targets to
1006 Differentially Regulate the Kinetochore-Microtubule Interface. *Mol. Cell* **38**, 383–392 (2010).
1007 55. Gergely, F. *et al.* The TACC domain identifies a family of centrosomal proteins that can
1008 interact with microtubules. *Proc. Natl. Acad. Sci.* **97**, 14352–14357 (2000).
1009
1010

1011 **Figure legends**

1012 **Figure 1: Proteomic screening reveals BOD1L1 as a mediator of UMK57 adaptation**

1013 A) Cartoon illustration depicting the experimental scheme used to discover mediators of
1014 UMK57 adaptation. SW620 cells were first treated for 3 days with UMK57 or DMSO
1015 control. They were then synchronized by thymidine-nocodazole treatment. The DMSO
1016 control sample was then treated with UMK57 for the final hour before harvest. The cells
1017 were then collected and analyzed by mass spectrometry.

1018 B) SW620 cells were prepared as in (A) but re-plated on glass coverslips instead of
1019 synchronization. After 24 hours, the cells were fixed and stained for Hec1 and DAPI. The
1020 rate of lagging chromosomes was then assessed. Statistical significance was calculated using
1021 Dunnett's multiple comparison test. Representative images from 3 independent experiments
1022 are shown. The images were adjusted evenly for brightness and contrast for presentation. The
1023 scale bar is 10μm.

1024 C) SW620 cells were prepared as in (A) and analyzed by mass spectrometry. The number of
1025 peptides and proteins detected in the screens are shown.

1026 D) Proteins from the phospho-proteomic screen that were significantly changed ($p < 0.1$) by
1027 Student's *t*-test were analyzed for gene ontology. The data were then transferred to Prism
1028 software and plotted.

1029 E) Proteins from the phospho-proteomic screen that were significantly changed ($p < 0.1$) by
1030 Student's *t*-test were analyzed by PhosphositePlus for sequence motif enrichment and
1031 plotted.

1032 F) Volcano plot analysis of the phospho-proteomic screen results. Proteins of potential interest
1033 are highlighted in orange. Statistical significance was calculated using two-tailed *t*-tests.

1034 G) Analysis of overlap between the phospho-proteomic study presented here and a previous
1035 study[14]. Proteins with changes in phosphorylation greater than 4-fold caused by Aurora A or
1036 Aurora B kinase inhibitors were considered targets of Aurora A or Aurora B kinase. The list
1037 of Aurora A and Aurora B targets was compared to the list of proteins from the phospho-
1038 proteomic screen that had a significantly changed phosphorylation site ($p < 0.1$) by Student's
1039 *t*-test.
1040 H) Cartoon drawing of the FAM44 protein family, showing the Bod1 similar domain and
1041 potential Aurora A kinase sites on BOD1L1. Scales are approximate.
1042 I) Amino acid sequence alignment of BOD1L1 orthologs from residues 2933-2992 (relative to
1043 the human sequence). Residues highlighted in pink indicate Aurora kinase defining motifs.
1044 Residues highlighted in yellow indicate potential phosphorylation sites.
1045 **Figure 2: BOD1L1 and Aurora A are required for adaptation to UMK57**
1046 A) SW620 cells were transfected with control shRNA or shRNA against BOD1L1 and selected
1047 with puromycin. Following selection, the cells were fixed and stained for Hec1 and DAPI.
1048 Control cells were treated with DMSO and cells adapted to UMK57 were treated for 72
1049 hours. Cells treated acutely with UMK57 were treated for 1 hour. The percentage of lagging
1050 chromosomes in anaphase for cells expressing the indicated shRNA is shown. 100 cells per
1051 shRNA and condition were scored for the presence of lagging chromosomes for each of 3
1052 independent biological repeats. Error bars indicate the mean +/- SEM. * denotes $p < 0.05$,
1053 *** denotes $p < 0.001$. Statistical significance was calculated between the indicated
1054 conditions using Dunnett's multiple comparison test.
1055 B) SW620 cells were transfected with control shRNA or shRNA against BOD1L1 and selected
1056 with puromycin. Following selection, the cells were fixed and stained for Hec1 and DAPI.

1057 Control cells were treated with DMSO, and cells adapted to UMK57 were treated for 72
1058 hours. Cells treated acutely with UMK57 were treated for 1 hour. The cells were then fixed
1059 and stained for Hec1 and DAPI. Representative images from 3 independent experiments are
1060 shown. The images were adjusted evenly for brightness and contrast for presentation. The
1061 scale bars of main images are 10 μm, and insets are 1 μm.

1062 C) SW620 cells were plated. 24 hours following plating, DMSO or 50 nM MLN8237 was
1063 added, with or without 100 nM UMK57. After 72 hours, the cells were fixed and stained for
1064 Hec1 and DAPI. The percentage of lagging chromosomes in anaphase for cells expressing
1065 the indicated shRNA is shown. 100 cells per shRNA and condition were scored for the
1066 presence of lagging chromosomes for each of 3 independent biological repeats. Error bars
1067 indicate the mean +/- SEM. * denotes $p < 0.05$, *** denotes $p < 0.001$. Statistical
1068 significance was calculated between the indicated conditions using Dunnett's multiple
1069 comparison test.

1070 D) SW620 cells were transfected with control shRNA or shRNA against BOD1L1 and selected
1071 with puromycin. Following selection, the cells were treated with DMSO or Okadaic acid as
1072 indicated for 90 minutes prior to fixation. The cells were then stained for Hec1 and DAPI.
1073 The percentage of lagging chromosomes in anaphase for cells expressing the indicated
1074 shRNA is shown. 100 cells per shRNA and condition were scored for the presence of lagging
1075 chromosomes for each of 3 independent biological repeats. Error bars indicate the mean +/-
1076 SEM. * denotes $p < 0.05$, *** denotes $p < 0.001$. Statistical significance was calculated
1077 between the indicated conditions using Dunnett's multiple comparison test.

1078 **Figure 3: Microtubule destabilization mediated by hyperactive MCAK enhances Aurora**
1079 **A/TPX2 localization to the mitotic spindle**

1080 A) Immunofluorescence images from an asynchronous population of SW620 cells treated either
1081 with DMSO control, acute (1 hour) UMK57 or UMK57 for 3 days. The cells were then fixed
1082 and stained for total Aurora A and Aurora A pT288. The Aurora A and Aurora A pT288
1083 were adjusted evenly for brightness and contrast for presentation. The DAPI channel of each
1084 condition was adjusted independently. Representative images from 2 independent biological
1085 experiments are shown. The scale bars are 10 μm.
1086 B) Quantification of the relative spindle protein intensities from the conditions from panel (A).
1087 The levels of the prometaphase DMSO conditions was set to 1 and the other conditions
1088 shown as fold-changes. The fluorescence levels for at least 30 cells for each of 2 independent
1089 biological repeats were measured. Error bars indicate the mean +/- SEM. Statistical
1090 significance was calculated between the indicated conditions using Dunnett's multiple
1091 comparison test.
1092 C) Cells were prepared as for panel (A) but stained for TPX2 and alpha tubulin.
1093 D) Cells were prepared as for panel (A) but stained for TACC3 and tubulin.
1094 E) Quantification of the relative spindle protein intensities from panels (C) and (D). The tubulin
1095 intensities from panels (C) and (D) were combined into a single plot.
1096 **Figure 4: BOD1L1 localizes to the mitotic spindle and kinetochores during mitosis**
1097 A) Immunofluorescence images from an asynchronous population of SW620 cells in various
1098 stages of mitosis stained for BOD1L1, Hec1 and DAPI. The BOD1L1 and Hec1 channels
1099 were adjusted evenly for brightness and contrast for presentation. The DAPI channel of each
1100 condition was adjusted independently. Representative images from 2 independent biological
1101 experiments are shown. The scale bars of main images are 10 μm, and insets are 1 μm.

1102 B) Immunofluorescence images from an asynchronous population of SW620 cells in various
1103 stages of mitosis stained for BOD1L1, alpha tubulin and DAPI. The BOD1L1 and alpha
1104 tubulin channels were adjusted evenly for brightness and contrast for presentation. The DAPI
1105 channel of each condition was adjusted independently. Representative images from 2
1106 independent biological experiments are shown. The scale bars of main images are 10 μm,
1107 and insets are 1 μm.
1108 C) Immunofluorescence images from an asynchronous population of SW620 cells in various
1109 stages of mitosis stained for BOD1L1, Aurora A and DAPI. The BOD1L1 and Hec1
1110 channels were adjusted evenly for brightness and contrast for presentation. The DAPI
1111 channel of each condition was adjusted independently. Representative images from 2
1112 independent biological experiments are shown. The scale bars of main images are 10 μm,
1113 and insets are 1 μm.
1114 **Figure 5: BOD1L1 is required for correct k-MT attachment stability and faithful**
1115 **chromosome segregation**
1116 A) Immunofluorescence images of SW620 cells were transfected with control shRNA or shRNA
1117 against BOD1L1 and selected with puromycin. The cells were then fixed and stained for
1118 alpha tubulin and ACA. Representative images of 2 independent biological experiments are
1119 shown. The images were adjusted evenly for brightness and contrast for presentation. The
1120 scale bar is 10μm.
1121 B) Quantification of the cells shown in panel (A). Statistical significance was calculated
1122 between the indicated conditions using Dunnett's multiple comparison test.
1123 C) SW620 cells were co-transfected with control shRNA or shRNA against BOD1L1 together
1124 with mCherry-H2B and selected with puromycin. Following selection, time lapse imaging

1125 was started at 5-minute intervals. The fate of at least 40 cells per experiment for each of 3
1126 independent biological repeats was recorded. Statistical significance was calculated between
1127 the indicated conditions using Dunnett's multiple comparison test.

1128 D) Immunofluorescence images of SW620 cells were transfected with control shRNA or shRNA
1129 against BOD1L1 and selected with puromycin. The cells were then placed at 4ºC for 15
1130 minutes before they were fixed and stained for alpha tubulin and ACA. Representative
1131 images of 3 independent biological experiments are shown. The images were adjusted evenly
1132 for brightness and contrast for presentation. The scale bar is 10μm.

1133 E) Quantification of the relative intensity of alpha Tubulin from the conditions shown in panel
1134 (D). The levels of prometaphase shC expressing cells were set to 1 and the other conditions
1135 shown as a fold-change. At least 50 cells per condition from each of 3 independent biological
1136 experiments were quantified. Error bars indicate the mean +/- SEM. **** denotes $p <$
1137 0.0001. Statistical significance was calculated between the indicated conditions using
1138 Dunnett's multiple comparison test.

1139 **Figure 6: BOD1L1 interacts with the PP2A-B56 phosphatase complex**

1140 A) Cartoon illustration depicting the experimental scheme used to discover protein interactors of
1141 BOD1L1. SW620 cells were first synchronized by thymidine-nocodazole. BOD1L1 was then
1142 immunoprecipitated and purified along with interacting proteins. The samples were then
1143 separated by SDS-PAGE. The entire lanes were excised and cut into 5 pieces and analyzed
1144 by mass spectrometry. The experiment was performed once.

1145 B) Table of selected interacting proteins detected in the control immunoprecipitation and
1146 BOD1L1 immunoprecipitations showing the number of detected peptides.

1147 C) SW620 cells were prepared as in panel (A), except that they were analyzed by Western blot.
1148 BOD1L1 was immunoprecipitated and the purified proteins were then separated by SDS-
1149 PAGE, transferred to nitrocellulose membrane and blotted as indicated. The panels were
1150 adjusted for brightness and contrast for presentation. An experiment representative of two
1151 independent biological repeats is shown.
1152 D) SW620 mitotic nuclear cell extracts were incubated with GST or GST-BOD1L fragments.
1153 Complexes were then isolated by glutathione-sepharose and analyzed by Western blot. The
1154 blot shown is representative of 2 independent experiments.
1155 **Figure 7: BOD1L1 expression is required for normal kinetochore phosphorylation**
1156 A) Immunofluorescence images from an asynchronous population of SW620 cells transfected
1157 with control shRNA or shRNA against BOD1L1 in prometaphase or metaphase and stained
1158 for Hec1, Hec1 pT31 and DAPI. The BOD1L1 and Hec1 channels were adjusted evenly for
1159 brightness and contrast for presentation. The DAPI channel of each condition was adjusted
1160 independently. Representative images from 2 independent biological experiments are shown.
1161 The scale bars of main images are 10 μm, and insets are 1 μm.
1162 B) As for panel (A), except for KNL1 pMELT/ACA instead of Hec1 pT31/total Hec1
1163 C) Quantification of the relative kinetochore pT31 Hec1/Hec1 intensities from the conditions
1164 from panel (A). The condition with the lowest level of pT31 Hec1/Hec1 was set to 1 and the
1165 other conditions shown as fold-changes. 25 kinetochores were quantified from each of 20
1166 cells for each of 2 independent biological repeats. Error bars indicate the mean +/- SEM.
1167 Statistical significance was calculated between the indicated conditions using Dunnett's
1168 multiple comparison test.
1169 D) As for panel (C), except for Hec1 pS44/total Hec1instead of Hec1 pT31/total Hec1

1170 E) As for panel (C), except for Hec1 pS55/total Hec1 instead of Hec1 pT31/total Hec1

1171 F) As for panel (C), except for DSN1 pS109/ACA instead of Hec1 pT31/total Hec1

1172 G) As for panel (C), except for KNL1 pMELT/ACA instead of Hec1 pT31/total Hec1

1173 H) As for panel (C), except for MCAK pS95/ACA instead of Hec1 pT31/total Hec1

1174 I) As for panel (C), except for Aurora B pT232/ACA instead of Hec1 pT31/total Hec1

1175 J) Quantification of total cellular Aurora A pT288/Total Aurora A. The condition with the
1176 lowest level of pT31 Hec1/Hec1 was set to 1 and the other conditions shown as fold-changes.
1177 The level of protein was measured from at least 25 cells for each of 2 independent biological
1178 repeats. Error bars indicate the mean +/- SEM. Statistical significance was calculated
1179 between the indicated conditions using Dunnett's multiple comparison test.

1180 **Figure 8: BOD1L1 is mutated in human cancers**

1181 A) The 10,967 sequenced cancers in the TCGA were queried for the presence of mutations in
1182 the *BOD1L1* gene and plotted by cancer subtype.

1183 B) Kaplan-Meier five-year overall survival by *BOD1L1* alteration status with Cox-Proportional
1184 Hazards Ratios and 95% confidence intervals from models adjusted for potential confounders
1185 (age, sex [except uterine], and tumor grade or stage). A) Uterine corpus endometrial
1186 carcinoma TCGA-UCEC, n= 529; b) lung adenocarcinoma TCGA-LUAD, n = 667; c)
1187 cutaneous melanoma TCGA-SKCM, n = 448; d) stomach adenocarcinoma TCGA-STAD, n
1188 = 440; e) lung squamous cell carcinoma TCGA-LUSC, n = 487.

1189 C) U2OS, HCT116, SW620 and HeLa cells were plated. They were then transfected with
1190 control shRNA or shRNA against BOD1L1 and selected with puromycin in the presence of
1191 compounds as indicated. After 1 week of selection, the cells were fixed and stained with

1192 crystal violet. Representative images from 3 independent experiments are shown. The scale
1193 bar is 4 cm.
1194 D) Quantification of cells from (C). The staining intensity of the cells was measured using Fiji
1195 and plotted. Error bars indicate the mean +/- SEM. Statistical significance was calculated
1196 between the indicated conditions using Student's *t*- test.
1197 E) Cartoon illustration showing a possible mechanism for adaptation to UMK57. UMK57
1198 agonizes MCAK, resulting in lower k-MT stability, which is sensed by Aurora A. Aurora A
1199 then phosphorylates BOD1L1, releasing PP2A to reduce phosphorylation of the NDC80
1200 complex, resulting in higher k-MT stability.
1201 **Figure S1: Changes in UMK57 adapted cells; Adaptation to UMK57 does not happen**
1202 **through changes to protein level**
1203 A) SW620 cells were first treated for 3 days with UMK57 or DMSO control. They were then re-
1204 plated on glass coverslips. After 24 hours, the cells were fixed and stained for Aurora B
1205 pT232, ACA and DAPI. A single experiment was performed. The scale bar is 10µm.
1206 B) SW620 cells were prepared as in (A) but stained for MCAK pS95 and ACA. A single
1207 experiment was performed. The scale bar is 10µm.
1208 C) Quantification of the relative kinetochore pT232 Aurora B/ACA intensities from the
1209 conditions from panel (A). The condition with the lowest level of pT232 Aurora B/ACA was
1210 set to 1 and the other conditions shown as fold-changes. 30 kinetochores were quantified
1211 from each of 20 cells from a single experiment. Error bars indicate the mean +/- SEM.
1212 Statistical significance was calculated between the indicated conditions using Dunnett's
1213 multiple comparison test.

1214 D) As for C but quantifying the relative kinetochore pS95 MCAK/ACA intensities from panel
1215 (B).
1216 E) Volcano plot analysis of the total protein level proteomic screen results. Proteins of potential
1217 interest are highlighted in orange. Statistical significance was calculated using two-tailed *t*-
1218 tests.
1219 F) STRING analysis of the statistically significant ($p < 0.1$) top-100 positively changed
1220 phosphorylated proteins and top-100 negatively changed phospho-proteins showing gene
1221 association networks.
1222 G) SW620 cells were first treated for 3 days with UMK57 or DMSO control. They were then
1223 allowed to remain asynchronous or were synchronized by thymidine-nocodazole. The cells
1224 were then harvested and lysed. The proteins were separated by SDS-PAGE, transferred to
1225 nitrocellulose membrane and finally blotted as indicated. The shown blots are representative
1226 of 3 independent experiments.
1227 **Figure S2: Validation of BOD1L1 antibody and shRNAs; BOD1L1 does not require**
1228 **Aurora A, Aurora B signaling or microtubules for kinetochore localization**
1229 A) SW620 cells were transfected with control shRNA or shRNA against BOD1L1 and selected
1230 with puromycin. The cells were then harvested at the indicated time points, lysed and the
1231 proteins separated by SDS-PAGE. They were then transferred to nitrocellulose membrane
1232 and blotted as indicated.
1233 B) Immunofluorescence images from an asynchronous population of SW620 transfected with
1234 control shRNA or shRNA against BOD1L1 and selected with puromycin. The cells were
1235 stained for BOD1L1, Hec1 and DAPI. The BOD1L1 and Hec1 channels were adjusted
1236 evenly for brightness and contrast for presentation. The DAPI channel of each condition was

1237 adjusted independently. Representative images from 2 independent biological experiments
1238 are shown. The scale bars of main images are 10 μm, and insets are 1 μm.
1239 C) SW620 cells were plated. 24 hours following plating, various concentrations of MLN8237
1240 were added as indicated. Following 3 days of treatment, the cells were fixed and stained with
1241 crystal violet. Representative images from 2 independent experiments are shown. The scale
1242 bar is 4 cm.
1243 D) Immunofluorescence images from an asynchronous population of SW620 transfected with
1244 control shRNA or shRNA against BOD1L1 and selected with puromycin. The cells were
1245 overnight with the indicated concentrations of nocodazole. The cells were then fized and
1246 stained for BOD1L1, Hec1 and DAPI. The BOD1L1 and Hec1 channels were adjusted
1247 evenly for brightness and contrast for presentation. The DAPI channel of each condition was
1248 adjusted independently. Representative images from 2 independent biological experiments
1249 are shown. The scale bars of main images are 10 μm, and insets are 1 μm.
1250 E) Immunofluorescence images from an asynchronous population of SW620 transfected with
1251 control shRNA or shRNA against BOD1L1 and selected with puromycin. The cells were
1252 then treated with DMSO control or Aurora A or Aurora B inhibitors for 90 minutes prior to
1253 fixation. The cells were stained for BOD1L1, Hec1 and DAPI. The BOD1L1 and Hec1
1254 channels were adjusted evenly for brightness and contrast for presentation. The DAPI
1255 channel of each condition was adjusted independently. Representative images from 2
1256 independent biological experiments are shown. The scale bars of main images are 10 μm,
1257 and insets are 1 μm.
1258 **Figure S3: Still images of live-cell movies; Hec1 is not required for BOD1L1 localization to**
1259 **kinetochores**

1260 A) SW620 cells were co-transfected with control shRNA or shRNA against BOD1L1 together
1261 with mCherry-H2B and selected with puromycin. After 72 hours of selection, time lapse
1262 imaging was started at 5-minute intervals. Representative Images from 3 independent
1263 experiments are shown. The images were independently adjusted for brightness and contrast
1264 for presentation. The scale bars are 10 μm.
1265 B) HeLa cells were plated on glass coverslips. 24 hours after plating, doxycycline or water was
1266 added to the wells. 48 hours following addition of doxycycline, the cells were fixed and
1267 stained as indicated. Representative Images from 2 independent experiments are shown. The
1268 images were independently adjusted for brightness and contrast for presentation. The scale
1269 bars of main images are 10 μm, and insets are 1 μm.
1270 **Figure S4: Overexpression of GFP-BOD1L1 rescues depletion of BOD1L1.**
1271 A) SW620 cells were plated. They were then transfected as indicated. 24 hours following
1272 transfection, puromycin was added. The cells were harvested 72 hours after transfection and
1273 lysed. The proteins were separated by SDS-PAGE, transferred to nitrocellulose membrane
1274 and finally blotted as indicated. A single experiment was performed.
1275 B) SW620 cells were plated on glass coverslips. They were then transfected as indicated. 24
1276 hours following transfection, puromycin was added. 72 hours following transfection, the cells
1277 were fixed and stained as indicated. Representative Images from 2 independent experiments
1278 are shown. The images were independently adjusted for brightness and contrast for
1279 presentation, except for DAPI, which was adjusted independently. The scale bars of main
1280 images are 10 μm, and insets are 1 μm.
1281 C) As for (B), but stained as indicated.

1282 D) RPE1 cells were plated on glass coverslips. They were then transduced with lentivirus as
1283 indicated. 24 hours following transduction, puromycin was added. 72 hours following
1284 transduction, the cells were fixed and stained as indicated. Representative Images from 2
1285 independent experiments are shown. The images were independently adjusted for brightness
1286 and contrast for presentation, except for DAPI, which was adjusted independently. The scale
1287 bars of main images are 10 μm, and insets are 1 μm.
1288 E) As for D but stained as indicated
1289 F) Quantification of the relative kinetochore pT31 Hec1/Hec1 intensities from the conditions
1290 from panel (B). The condition with the lowest level of pT31 Hec1/Hec1 was set to 1 and the
1291 other conditions shown as fold-changes. 25 kinetochores were quantified from each of 20
1292 cells for each of 2 independent biological repeats. Error bars indicate the mean +/- SEM.
1293 Statistical significance was calculated between the indicated conditions using Dunnett's
1294 multiple comparison test
1295 G) Quantification of the relative kinetochore KNL1 pMELT intensities from panel (C) as for
1296 panel (F).
1297 H) Quantification of the relative pT31 Hec1/Hec1 intensities from the conditions from panel (D)
1298 as for panel (F). 25 kinetochores were quantified from at least 22 cells over two independent
1299 biological repeats.
1300 I) Quantification of the relative KNL1 pMELT intensities from panel (E) as for panel (F). 25
1301 kinetochores were quantified from at least 27 cells over two independent biological repeats.
1302 **Figure S5: Mutations in BOD1L1 are mutually exclusive from mutations in other pathway**
1303 **components.**

1304 A) The 10,967 sequenced cancers in the TCGA were queried for the presence of mutations in
1305 the *BOD1L1*, *Aurora A, TPX2, PPP2CA, PPP2CB, PPP2R1A, PPP2R1B, PPP2R5A,*
1306 *PPP2R5B, PPP2R5C, PPP2R5D, PPP2R5E* genes and plotted by cancer subtype.
1307 B) The 10,967 sequenced cancers in the TCGA were queried for the presence of mutations in
1308 *BOD1L1*, *Aurora A, TPX2, PPP2CA, PPP2CB, PPP2R1A, PPP2R1B, PPP2R5A, PPP2R5B,*
1309 *PPP2R5C, PPP2R5D, PPP2R5E* and plotted showing the overlap of alterations.
1310 C) Mutual exclusivity between genes in *BOD1L1* and the other queried genes was tested by
1311 *BOD1L1* alteration versus alteration to any other gene pathway member (Fisher's exact
1312 P=1.3E-24), and *BOD1L1* alteration versus each of the eleven gene pathway members
1313 independently.
1314 D) U2OS, HCT116, SW620 and HeLa cells were plated. They were then transfected with
1315 control shRNA or shRNA against BOD1L1. 24 hours post-transfection, puromycin was
1316 added. 72 hours after addition of puromycin, the cells were harvested by scraping and lysed.
1317 The proteins were then separated by SDS-PAGE and transferred to nitrocellulose membrane
1318 and finally blotted as indicated.
1319 E) U2OS, HCT116, HEC1 and HeLa cells were plated. They were then transfected with control
1320 shRNA or shRNA against BOD1L1 and selected with puromycin. After 3 days of selection,
1321 the cells were fixed and stained with Hec1 and DAPI and the rates of lagging chromosomes
1322 were assessed from100 anaphases for each 3 independent experiments. Error bars indicate
1323 the mean +/- SEM. Statistical significance was calculated between the indicated conditions
1324 using Student's *t*- test.
1325 F) U2OS or SW620 cells were plated. They were then transfected with control shRNA or
1326 shRNA against BOD1L1 and selected with puromycin. After 3 days of selection, the cells

1327 were fixed and stained with Hec1 and DAPI and the percentage of cells with micronuclei was
1328 determined. At least 1000 cells were examined per condition for each 3 independent
1329 experiments. Error bars indicate the mean +/- SEM. Statistical significance was calculated
1330 between the indicated conditions using Student's *t*- test.

1331 G) Cells were prepared as in figure 7C. Following fixation, the cells were imaged by brightfield
1332 microscopy. Representative images of 3 independent experiments are shown. The scale bar is
1333 100 μm.

1334 **Figure S6: RPE1 cells are resistant to BOD1L1 knockdown.**

1335 A) RPE1 cells were plated. They were then transduced with lentivirus as indicated. 24 hours
1336 following transfection, puromycin was added. The cells were harvested 72 hours after
1337 transfection and lysed. The proteins were separated by SDS-PAGE, transferred to
1338 nitrocellulose membrane and finally blotted as indicated. A single experiment was
1339 performed.

1340 B) RPE1 cells were plated They were then transduced with control shRNA or shRNA against
1341 BOD1L1 and selected with puromycin in the presence of compounds as indicated. After 1
1342 week of selection, the cells were fixed and stained with crystal violet. Representative images
1343 from 3 independent experiments are shown. The scale bar is 4 cm.

1344 C) Cells were prepared as in figure 7C. Following fixation, the cells were imaged by brightfield
1345 microscopy. Representative images of 3 independent experiments are shown. The scale bar is
1346 100 μm.

1347 D) Quantification of cells from (B). The staining intensity of the cells was measured using Fiji
1348 and plotted. Error bars indicate the mean +/- SEM. Statistical significance was calculated
1349 between the indicated conditions using Student's *t*- test.

Kucharski et al. Figure 1

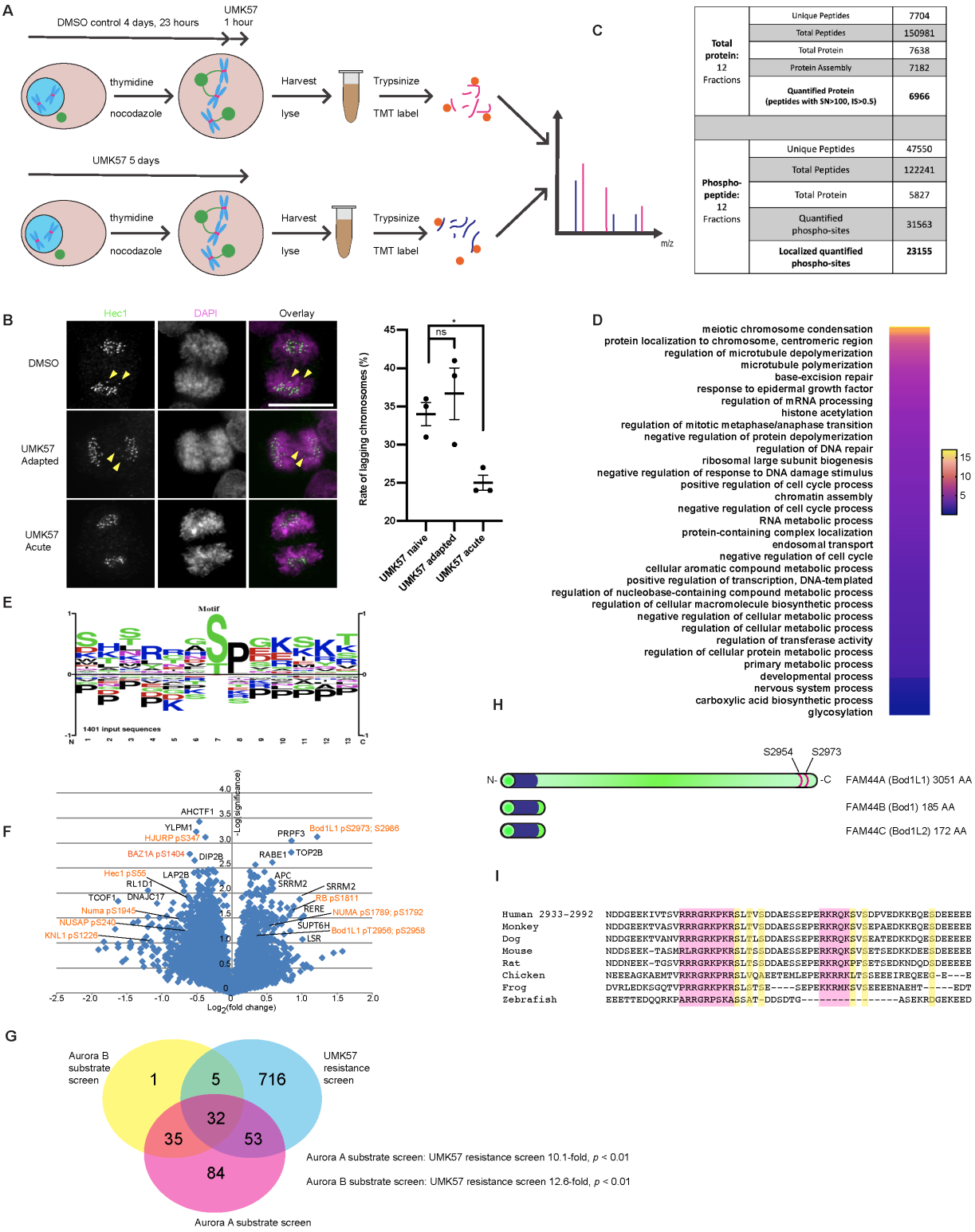

Kucharski et al. Figure S1

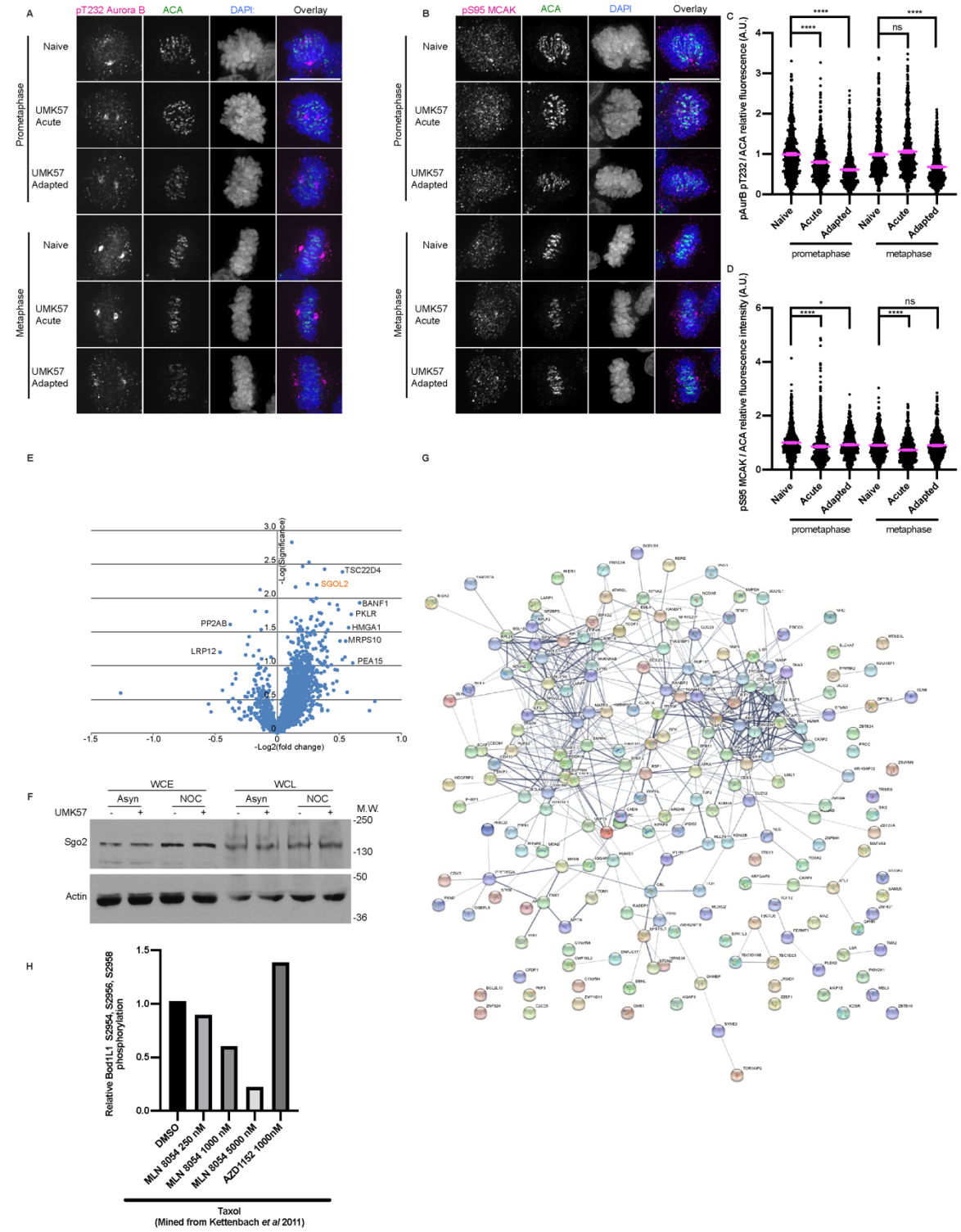

1351

1352

1353

Kucharski et al. Figure 2

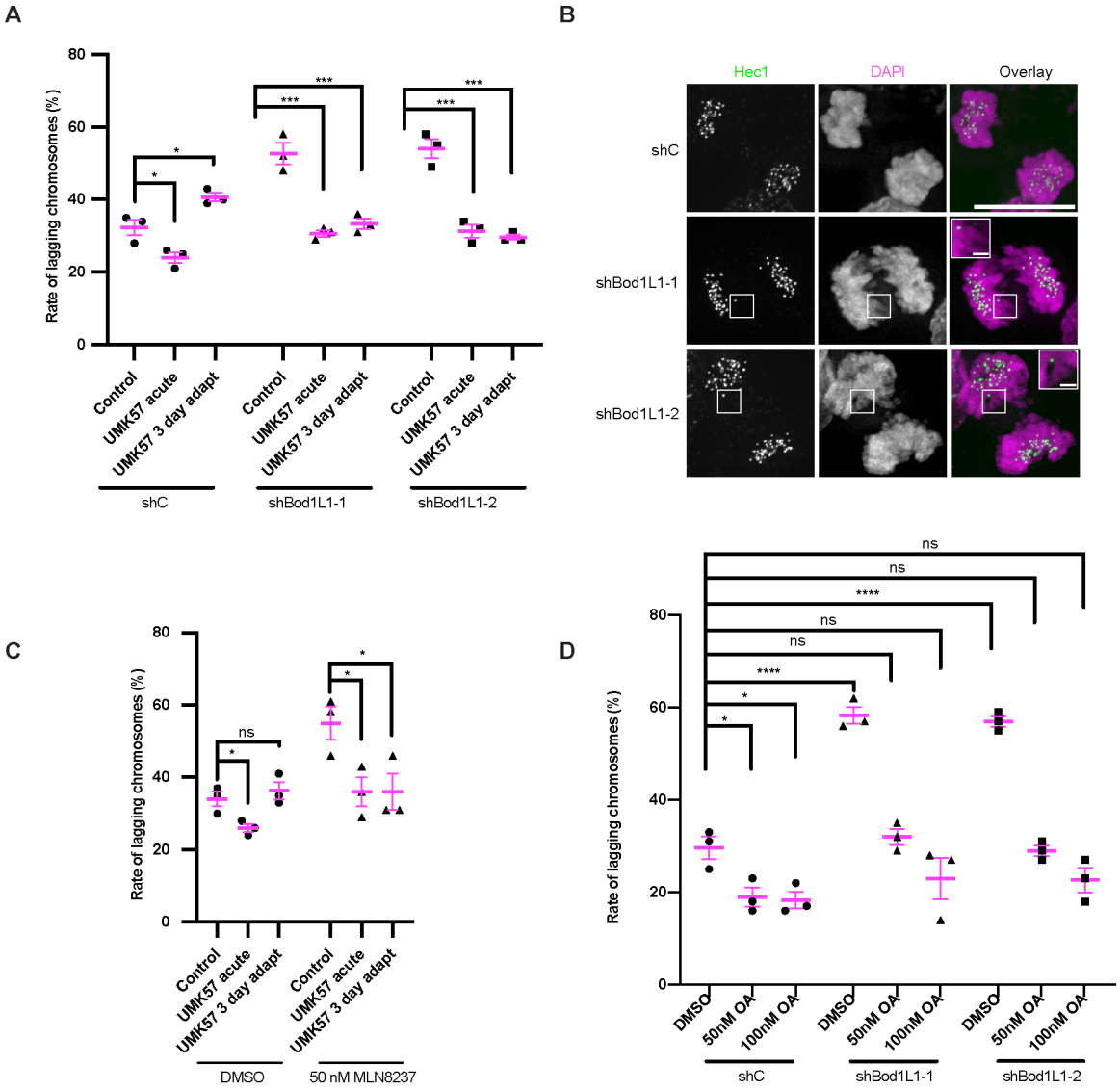

1354

1355

1356

Kucharski et al. Figure 3

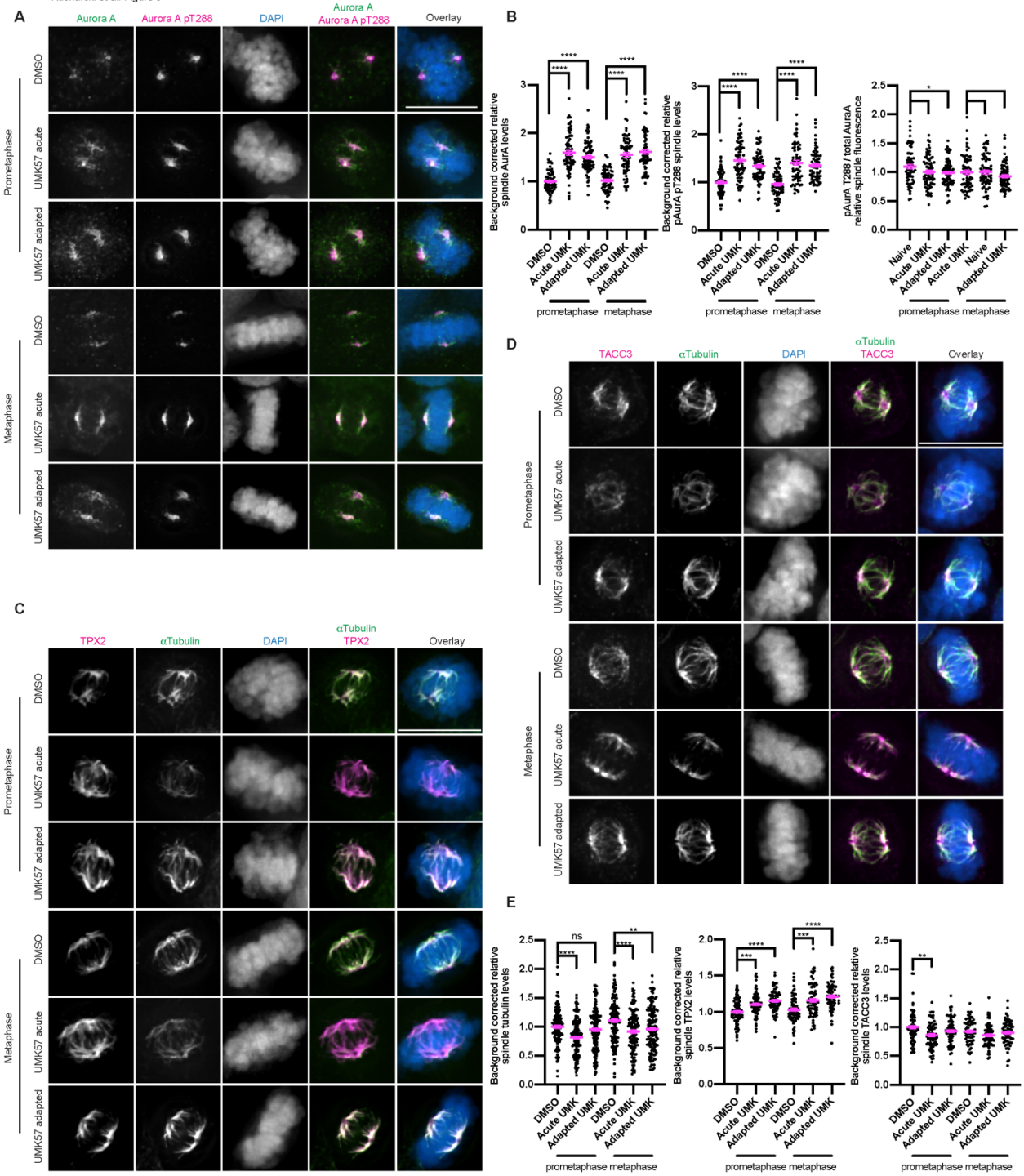

1357

Kucharski et al. Figure S2

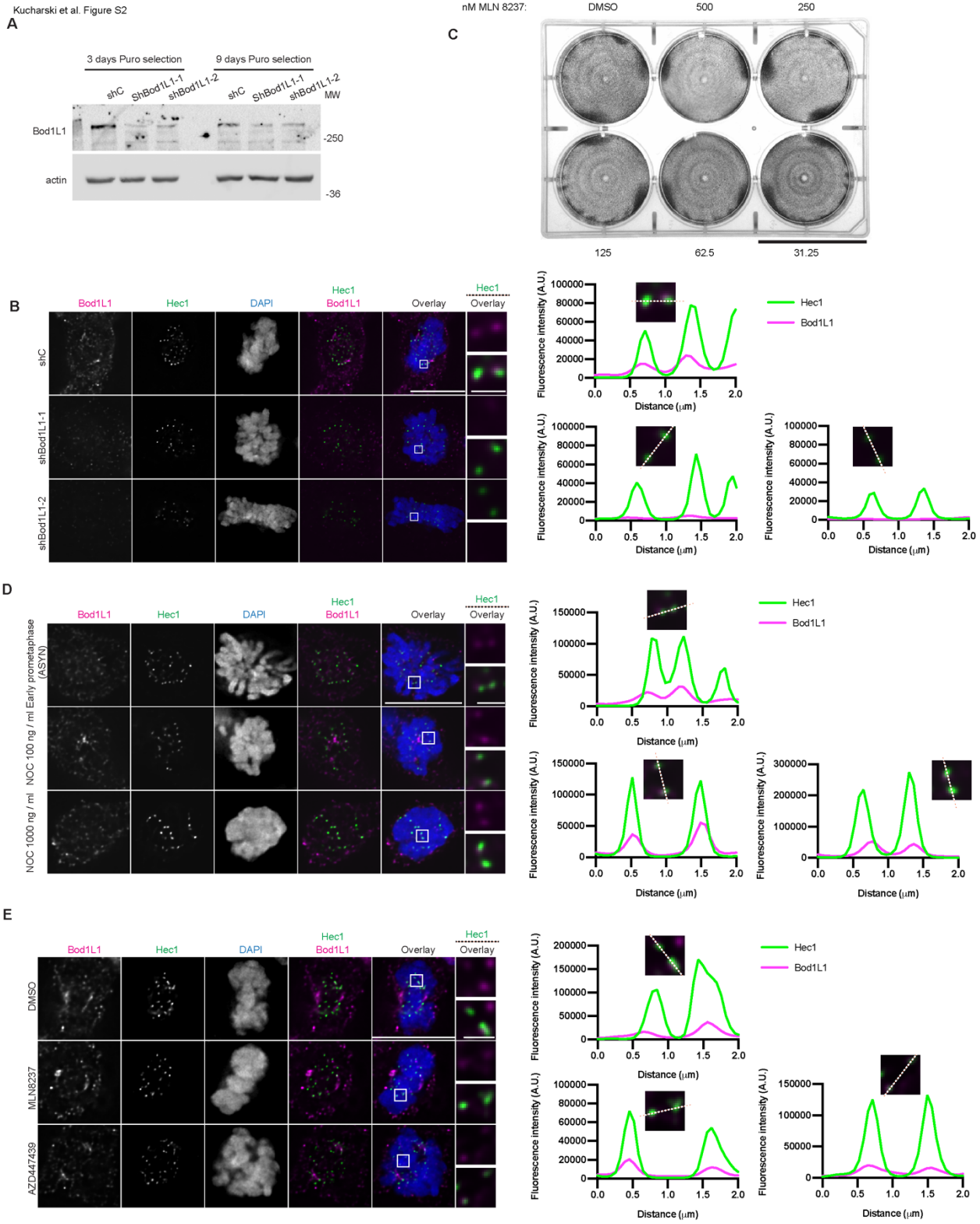

1358

1359

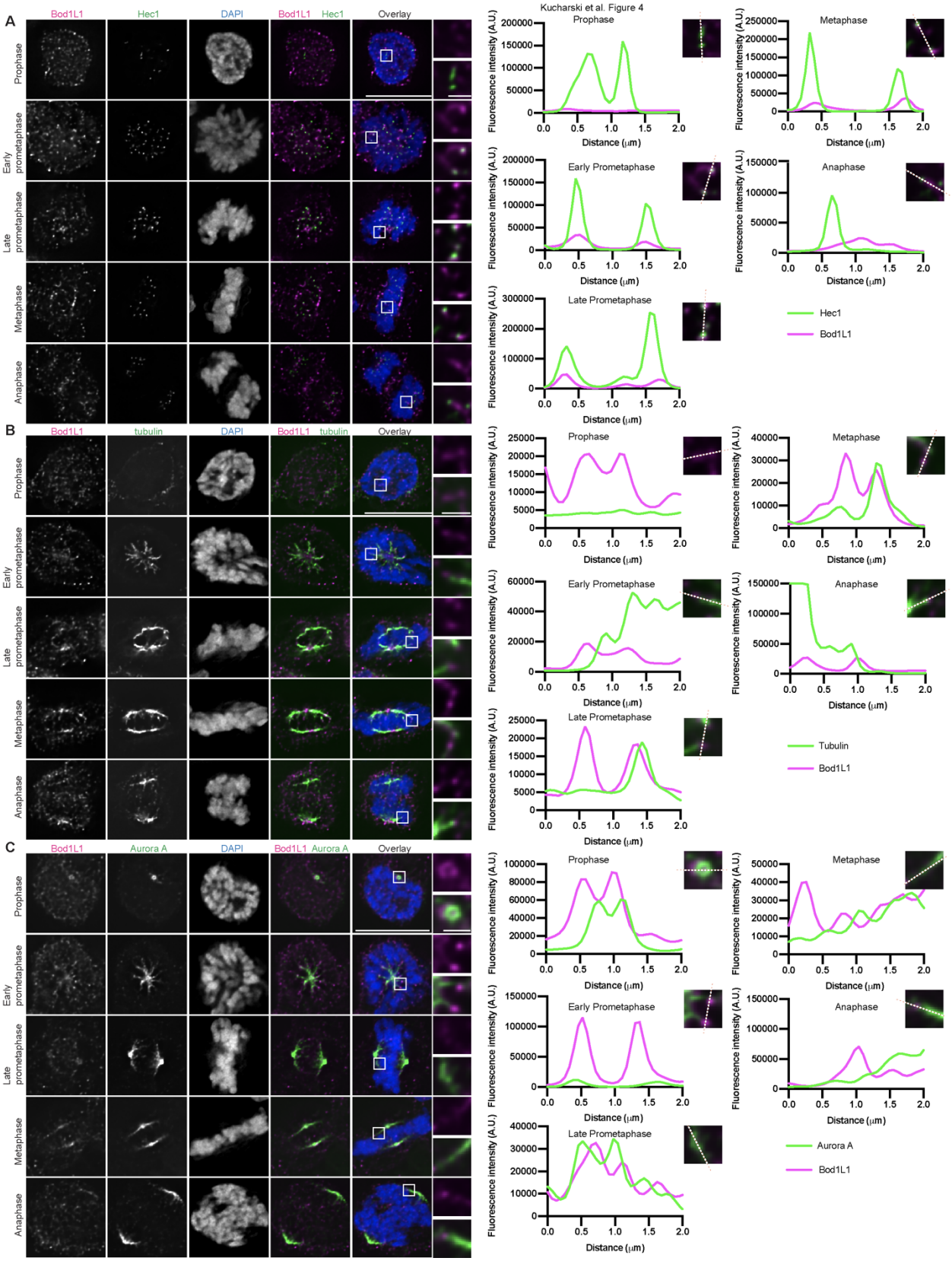
Kucharski et al. Figure 4
A
Bod1L1
Hec1
DAPI
Bod1L1 Hec1
Overlay
Prophase
Early prometaphase
Late prometaphase
Metaphase
Anaphase
Fluorescence intensity (A.U.)
Distance (μm)
Hec1
Bod1L1
B
tubulin
Bod1L1 tubulin
Tubulin
C
Aurora A
Bod1L1 Aurora A

1360

Kucharski et al. Figure 5

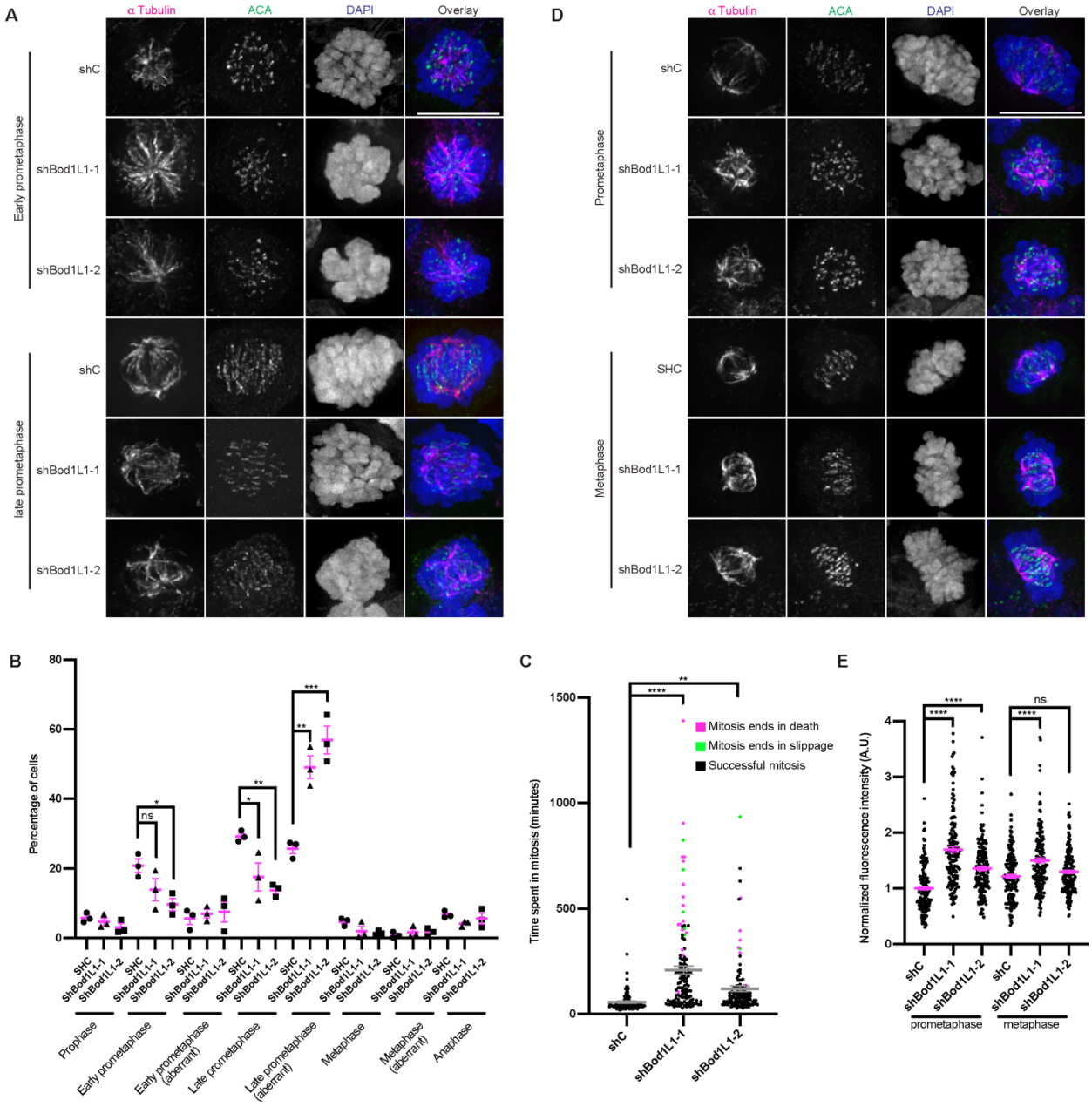

1361

Kucharski et al. Figure S3

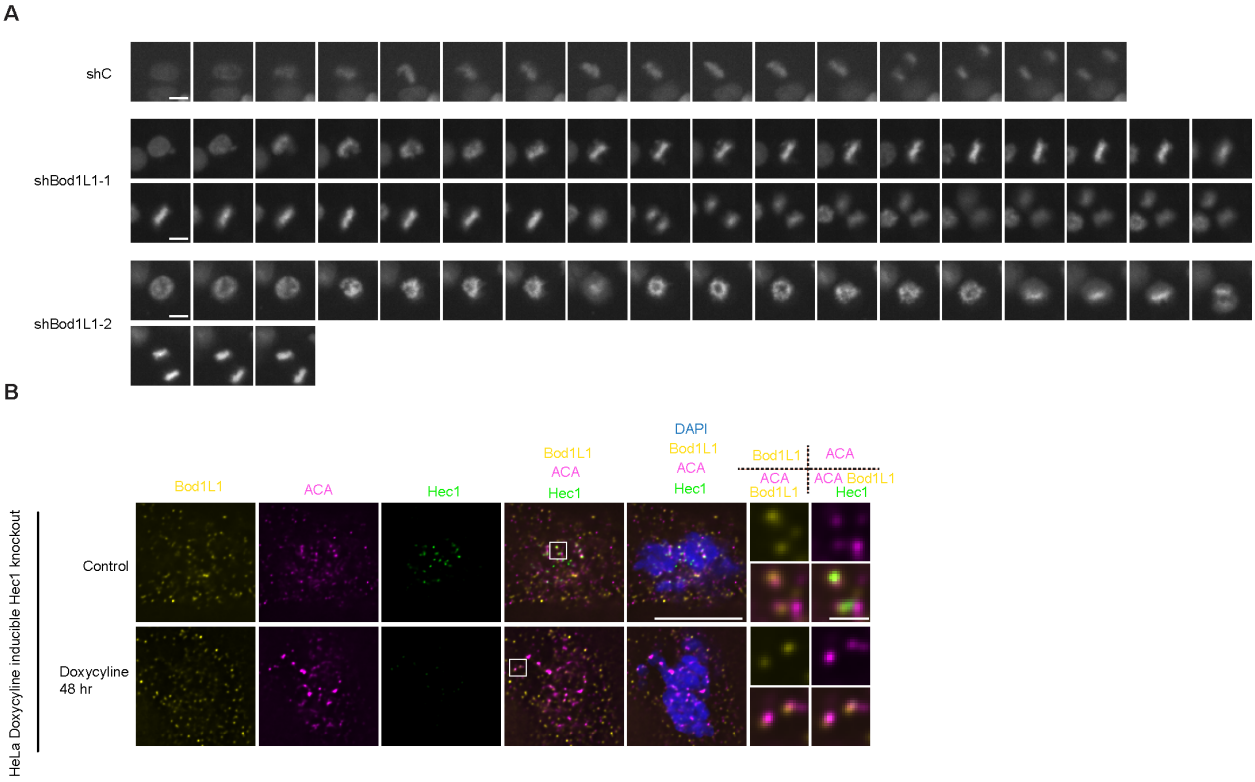

1362

Kucharski et al. Figure 6

A

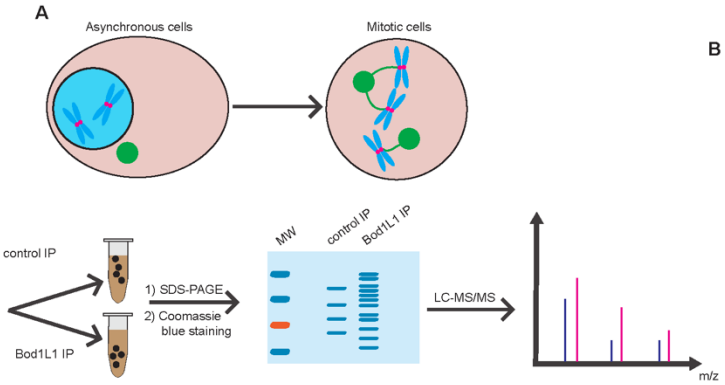

B

Protein ID	Number of peptides in control IP	Number of peptides in Bod1L1 IP
Bod1L1	0	62
Rictor	0	30
PRPF8	0	31
MAPKAP1	0	13
Sgo2	0	4
CENPF	0	6
MCAK	4	8
PP2R1A	2	15
PP2R1B	0	3
PP2CA	1	3
PP2R5E	0	5
Numa	0	5
AurKA	0	2
APC3	0	4
APC8	0	5

C

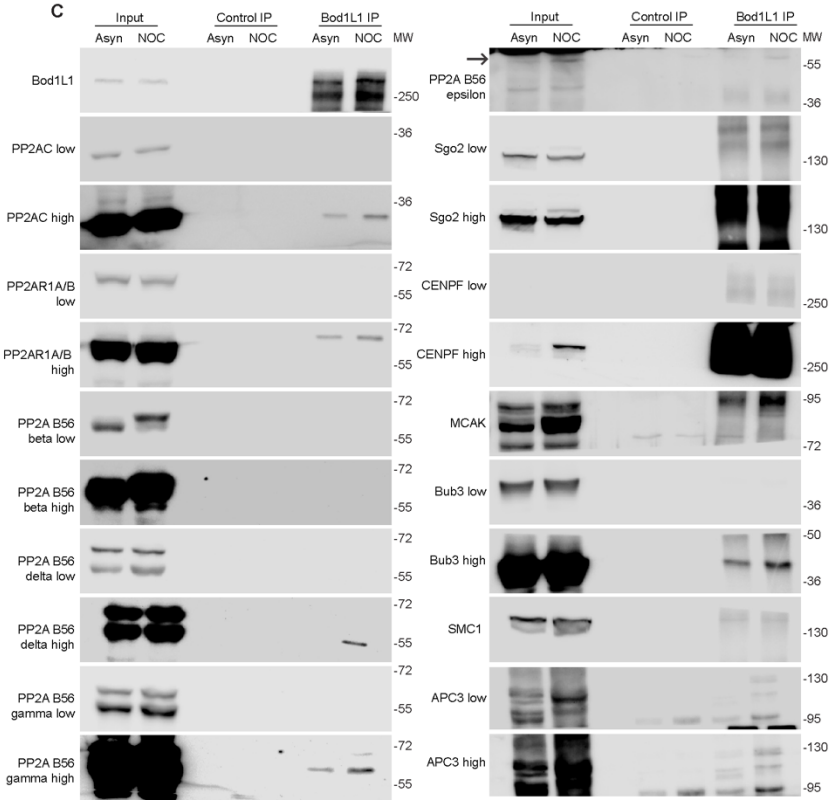

D

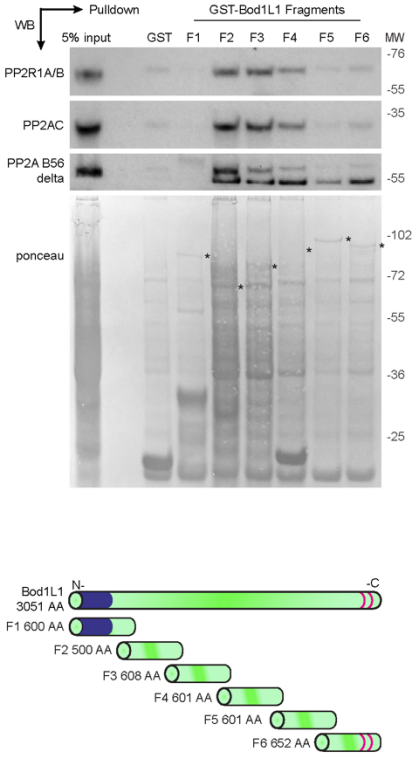

1363

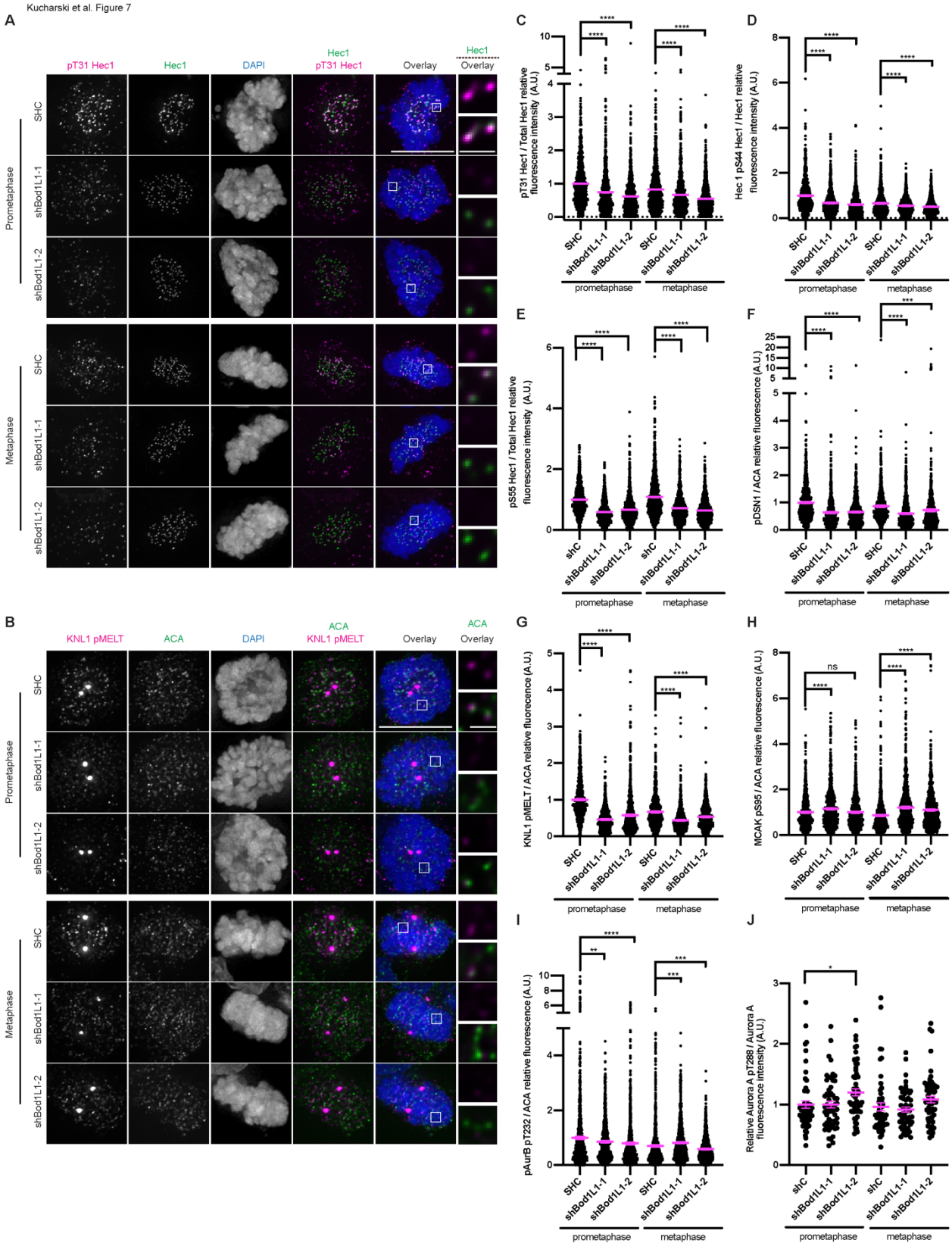
Kucharski et al. Figure 7
A
pT31 Hec1
Hec1
DAPI
Hec1
pT31 Hec1
Overlay
Hec1
Overlay
Prometaphase
Metaphase
SHC
shBod1L1-1
shBod1L1-2
B
KNL1 pMELT
ACA
DAPI
ACA
KNL1 pMELT
Overlay
ACA
Overlay
C
pT31 Hec1 / Total Hec1 relative fluorescence intensity (A.U.)
D
Hec 1 pS44 Hec1 / Hec1 relative fluorescence intensity (A.U.)
E
pS55 Hec1 / Total Hec1 relative fluorescence intensity (A.U.)
F
pDSN1 / ACA relative fluorescence (A.U.)
G
KNL1 pMELT / ACA relative fluorescence (A.U.)
H
MCAK pS95 / ACA relative fluorescence (A.U.)
I
pAurB pT232 / ACA relative fluorescence (A.U.)
J
Relative Aurora A pT288 / Aurora A fluorescence intensity (A.U.)
prometaphase
metaphase
ns

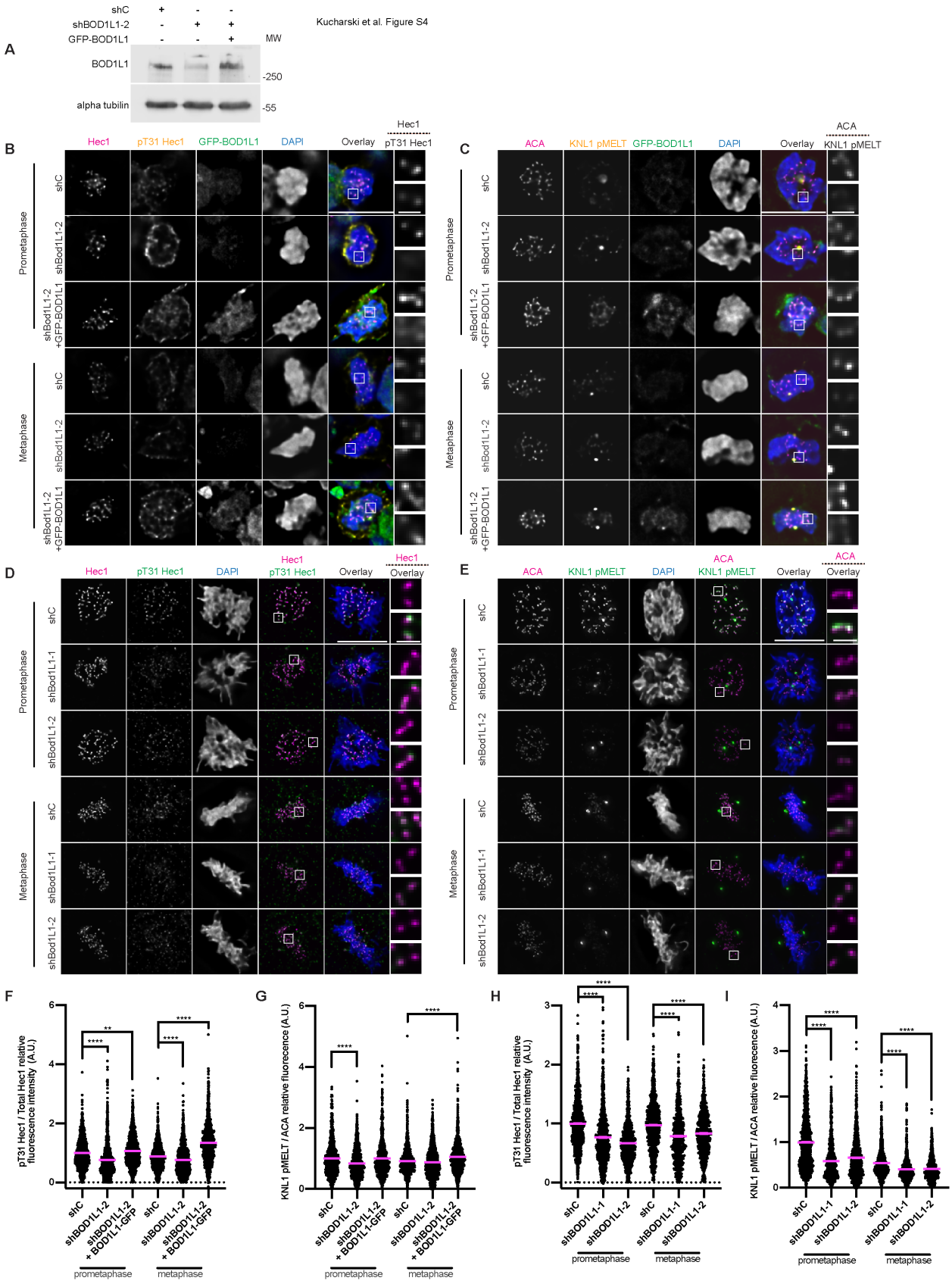
Kucharski et al. Figure S4
A
shC
shBOD1L1-2
GFP-BOD1L1
MW
BOD1L1
alpha tubilin
-250
-55
B
Hec1
pT31 Hec1
GFP-BOD1L1
DAPI
Overlay
Prometaphase
Metaphase
shC
shBod1L1-2
shBod1L1-2 +GFP-BOD1L1
C
ACA
KNL1 pMELT
D
shBod1L1-1
E
F
pT31 Hec1 / Total Hec1 relative fluorescence intensity (A.U.)
shBOD1L1-2 + BOD1L1-GFP
prometaphase
metaphase
G
KNL1 pMELT / ACA relative fluorescence (A.U.)
H
I

Kucharski *et al.* Figure 8

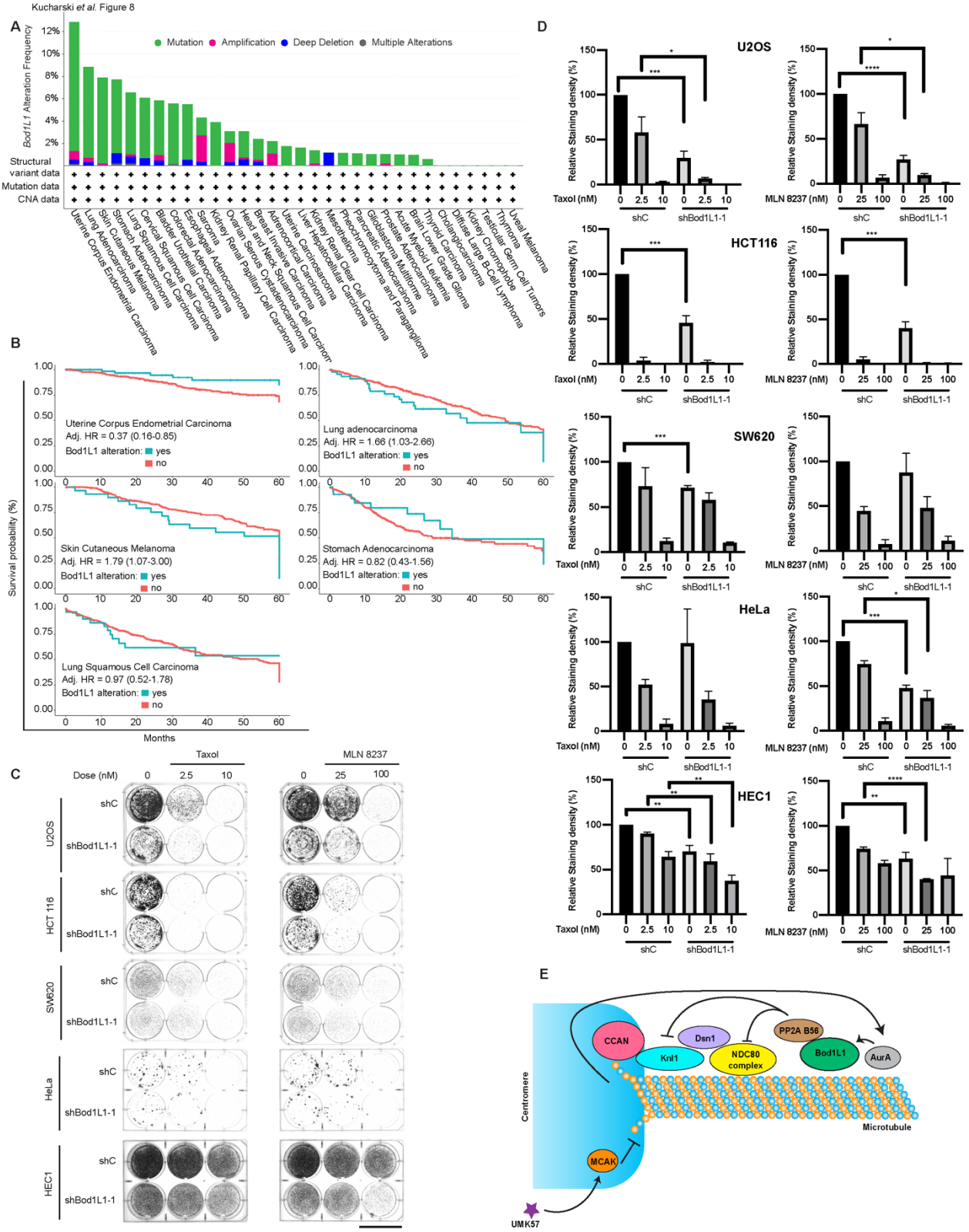

1366

1367

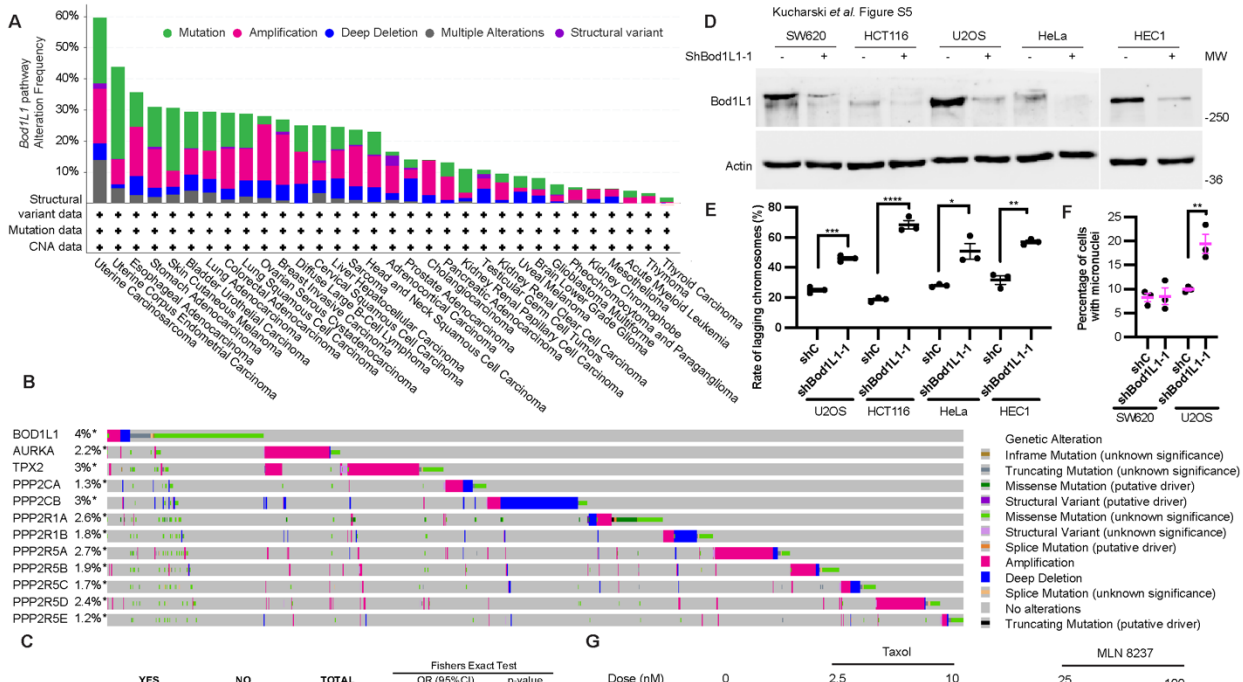

C

	YES	NO	TOTAL	Fishers Exact Test OR (95%CI)	p-value
Any Pathway Gene Altered					
YES	171 (1.56%)	257 (2.34%)	428 (3.9%)	2.99 (2.44-3.67)	1.26E-24
NO	1916 (17.47%)	8623 (78.63%)	10539 (96.1%)		
TOTAL	2087 (19.03%)	8880 (80.97%)	10967 (100%)		
Altered AURKA					
YES	27 (0.25%)	401 (3.66%)	428 (3.9%)	3.32 (2.12-5.05)	5.01E-07
NO	209 (1.91%)	10330 (94.19%)	10539 (96.1%)		
TOTAL	236 (2.1%)	10731 (97.9%)	10967(100%)		
Altered TPX2					
YES	47 (0.43%)	381 (3.47%)	428 (3.9%)	3.78(2.68 -5.24)	1.44E-12
NO	333 (3.04)	10206 (93.06 %)	10539 (96.1%)		
TOTAL	380 (3.47%)	10587 (96.53%)	10967 (100%)		
Altered PPP2CA					
YES	23 (0.21%)	405 (3.69%)	428 (3.9%)	4.89 (2.95-7.78)	7.49E-09
NO	121 (1.10%)	10418 (94.99 %)	10539 (96.1%)		
TOTAL	144 (1.31%)	10823 (98.68%)	10967 (100%)		
Altered PPP2CB					
YES	36 (0.33%)	392 (3.57%)	428 (3.9%)	3.06 (2.07-4.40)	5.66E-08
NO	307 (2.8%)	10232 (93.3%)	10539 (96.1%)		
TOTAL	343 (3.13%)	10624 (96.87%)	10967 (100%)		
Altered PPP2R1A					
YES	39 (0.36%)	389 (3.55%)	428 (3.9%)	4.14 (2.83-5.92)	7.99E-12
NO	249 (2.27%)	10290 (93.83%)	10539 (96.1%)		
TOTAL	288 (2.63%)	10679 (97.38%)	10967 (100%)		
Altered PPP2R1B					
YES	33 (0.30%)	395 (3.60%)	428 (3.9%)	5.09 (3.35-7.55)	2.25E-12
NO	170 (1.55%)	10369 (94.55%)	10539 (96.1%)		
TOTAL	203 (1.85%)	10764 (98.15%)	10967 (100%)		
Altered PPP2R5A					
YES	41 (0.37%)	387 (3.53%)	428 (3.9%)	4.29 (2.96-6.09)	9.45E-13
NO	254 (2.32%)	10285 (93.78%)	10539 (96.1%)		
TOTAL	295 (2.69%)	10672 (97.31%)	10967 (100%)		
Altered PPP2R5B					
YES	31 (0.28%)	397 (3.62%)	428 (3.9%)	4.44 (2.89-6.63)	1.96E-10
NO	182 (1.66%)	10357 (94.44%)	10539 (96.1%)		
TOTAL	213 (1.94%)	10754 (98.06%)	10967 (100%)		
Altered PPP2R5C					
YES	27 (0.25%)	401 (3.66%)	428 (3.9%)	4.54 (2.86-6.96)	1.73E-09
NO	154 (1.40%)	10385 (94.69%)	10539 (96.1%)		
TOTAL	181 (1.65%)	10786 (98.35%)	10967 (100%)		
Altered PPP2R5D					
YES	33 (0.30%)	395 (3.60%)	428 (3.9%)	3.68 (2.44-5.40)	3.77E-09
NO	234 (2.13%)	10305 (93.96%)	10539 (96.1%)		
TOTAL	267 (2.43%)	10700 (97.56%)	10967 (100%)		
Altered PPP2R5E					
YES	24 (0.22%)	404 (3.68%)	428 (3.9%)	5.53 (3.36-8.76)	4.33E-10
NO	112 (1.02%)	10427 (95.08%)	10539 (96.1%)		
TOTAL	136 (1.24%)	10831 (98.76%)	10967 (100%)		

Altered BOD1L1
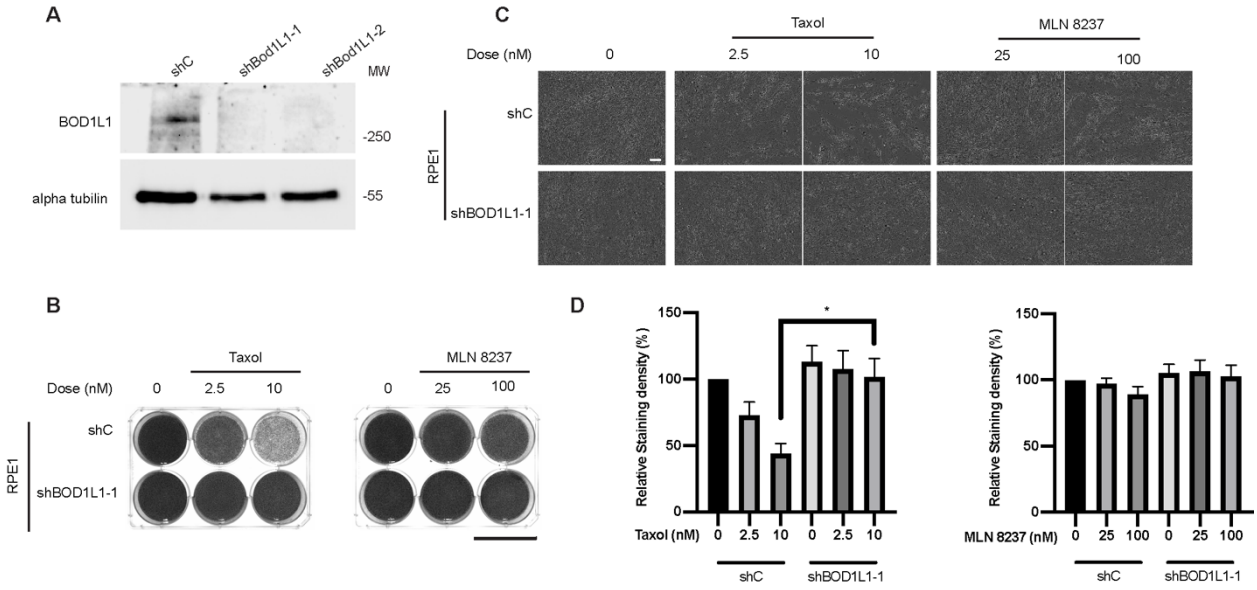
Kucharski *et al.* Figure S6